

SEMI-ANALYTICAL MODEL FOR THIN PLATE DYNAMICS

by

Joyson Stany Menezes

A thesis submitted to the faculty of
The University of North Carolina at Charlotte
in partial fulfillment of the requirements
for the degree of Master of Science in
Mechanical Engineering

Charlotte

2016

Approved by

Dr. Tony L. Schmitz

Dr. John C. Ziegert

Dr. Matthew A. Davies

ABSTRACT

JOYSON STANY MENEZES. Semi-analytical model for thin-plate dynamics.
(Under the direction of DR. TONY L. SCHMITZ)

Productivity when milling thin, monolithic components is often limited by regenerative chatter. The vibrations are partially controlled by the use of stability lobe diagrams, which enable the selection of spindle speed/axial depth combinations to avoid chatter. However, this requires knowledge of both the tool and structure dynamics.

The objective of this numerical study is to model the dynamics of thin-walled structures. A complete finite element analysis is carried out using ABAQUS/Standard. An analytical model is developed for the natural frequency and minimum lateral stiffness of thin plates with clamped-clamped-clamped-free boundary conditions. The stiffness is determined using the first (most flexible) transverse bending mode. The dynamic characteristics of the plate were predicted using finite element analysis and the accuracy was experimentally validated. Based on these studies, the predicted and measured natural frequency, stiffness values, and mode shapes showed good agreement. Using the numerical finite element modeling capability, the natural frequency and minimum stiffness for the first (most flexible) mode was evaluated over a range of lengths, thickness, and heights. The trends were combined into a look up table that can be used to identify the natural frequency and minimum rib stiffness for any selected geometry. Using the interpolated natural frequency and stiffness values, the workpiece dynamics can be defined and, using milling stability methods, stable machining parameters may be identified.

DEDICATION

I would like to dedicate my thesis to my loving parents, Janet and Stany Menezes, my brother Rohan, my mentor, Dr. Tony Schmitz, and all my friends.

ACKNOWLEDGEMENTS

I would like to thank my advisor, Dr. Tony Schmitz, for his patience, his ideas, and for providing the opportunity to participate in this experience. I have grown both professionally and personally under his guidance. I would also like to thank the other members of the supervisory committee, Dr. John Ziegert and Dr. Matthew Davies, for their participation.

I would also like to thank all the students and faculty of the Mechanical Engineering and Engineering Science department for making the research possible. Furthermore, I would like to specifically recognize Dr. Harish Cherukuri, Dr. Chris Tyler, Mark Rubeo and Kadir Kiran for their assistance and guidance throughout this effort.

Lastly, I thank all my family, roommates and friends for their continued support and encouragement.

TABLE OF CONTENTS

LIST OF FIGURES	viii
CHAPTER 1: INTRODUCTION	1
1.1 Thin-wall Machining	1
1.2 Literature Review	2
1.3 Research Objective and Scope	3
1.3.1 Case I: Thin-wall With Cantilever Boundary Condition	4
1.3.2 Case II: Thin-wall With CCCF Boundary Condition	5
CHAPTER 2: FINITE ELEMENT MODELING	7
2.1 Background	7
2.2 ABAQUS/Standard Overview	7
2.2.1 Preprocessing	8
2.2.2 Simulation	9
2.2.3 Postprocessing	9
2.2.4 Analysis Procedure	9
CHAPTER 3: EXPERIMENTAL VALIDATION	38
3.1 Experimental Setup	38
3.2 Comparison of Experimental and Measured Results	41
3.2.1 Mode Shapes	41

3.2.2 Frequency Response Function	44
3.2.3 Stiffness	46
3.3 Test Geometries	47
CHAPTER 4: RESULTS AND DISCUSSION	50
4.1 Repeatability	50
4.2 Mesh Density	51
4.3 Comparison with Analytical Natural Frequency	53
4.4 Grid and Interpolation for Natural Frequency and Stiffness	57
CHAPTER 5: SUMMARY AND CONCLUSION	61
REFERENCES	63
APPENDIX A: GRID AND INTERPOLATION FOR NATURAL FREQUENCY AND STIFFNESS MATLAB CODE	69

LIST OF FIGURES

FIGURE 1.1: Machining of a thin-wall workpiece with conventional tool (left) and relieved tool (right) [4].	2
FIGURE 1.2: Predicted first mode stiffness for different boundary conditions.	5
FIGURE 1.3: Predicted second mode stiffness for different boundary conditions.	6
FIGURE 2.1: ABAQUS analysis stages.	8
FIGURE 2.2: The Start Session dialog box.	10
FIGURE 2.3: Components of the main window.	10
FIGURE 2.4: The Create Part dialog box.	11
FIGURE 2.5: The Sketcher grid with a grid size of 0.1.	12
FIGURE 2.6: Two-dimensional (2D) detailed drawing of an aluminum Al-6061 thin-walled structure with cantilever boundary condition.	13
FIGURE 2.7: Sketching the horizontal and vertical center line on the Sketcher grid.	15
FIGURE 2.8: Sketching the base feature.	15
FIGURE 2.9: Sketching the constraints.	16
FIGURE 2.10: Base feature sketch with all dimensions and constraints.	16
FIGURE 2.11: Sketching the thin-wall feature.	17
FIGURE 2.12: Base and thin-wall feature sketch with all dimensions and constraints	17
FIGURE 2.13: The self-intersection zone between the base and thin-wall feature sketch.	18
FIGURE 2.14: Fully constrained sketch for the base and thin-wall feature.	18
FIGURE 2.15: Extruded solid 3D CAD model for a thin-wall structure with cantilever boundary condition.	19
FIGURE 2.16: Edit Material dialog box.	20

FIGURE 2.17: The Edit Section Assignment dialog box indicates that a section named Thin_wall_structure made of Aluminum-6061 will be assigned to the CAD model.	21
FIGURE 2.18: Al-6061 material properties assigned to thin-wall 3D CAD model.	21
FIGURE 2.19: The thin-wall with cantilever boundary condition with default mesh seed in mesh module.	24
FIGURE 2.20: Poor mesh quality of the with respect to the default mesh seeds with 420 elements.	24
FIGURE 2.21: Uniform mesh quality throughout the part with 672 nodes and 380 elements.	25
FIGURE 2.22: Effect of mesh refinement on natural frequency (left) and minimum stiffness (right).	26
FIGURE 2.23: FEM encastre boundary condition: the bottom face is constrained from all displacements and rotations.	27
FIGURE 2.24: Viewport window displaying the undeformed shape of the thin-wall structure with cantilever boundary condition.	28
FIGURE 2.25: Step/Frame dialog box displaying the mode and its corresponding frequency for thin-walled structure with cantilever boundary condition.	29
FIGURE 2.26: Predicted first mode shape, ψ_1 , with a natural frequency of 5605.2 Hz for the cantilever boundary condition.	30
FIGURE 2.27: Predicted second mode shape, ψ_2 , with a natural frequency of 6115 Hz for the cantilever boundary condition.	30
FIGURE 2.28: Predicted third mode shape, ψ_3 , with a natural frequency of 7668.5 Hz for the cantilever boundary condition.	31
FIGURE 2.29: Two-dimensional (2D) detailed drawing of an aluminum Al-6061 thin-walled structure with clamped-clamped-clamped-free (CCCF) boundary conditions.	32
FIGURE 2.30: Predicted first mode shape, ψ_1 , with a natural frequency of 5821.9 Hz for the CCCF boundary condition.	33
FIGURE 2.31: Predicted second mode shape, ψ_2 , with a natural frequency of 7598.1 Hz for the CCCF boundary condition.	33
FIGURE 3.1: Schematic representation of cantilever rib FRF measurement setup using an impact hammer and laser vibrometer.	39
FIGURE 3.2: Schematic representation of CCCF rib FRF measurement setup using an impact hammer and laser vibrometer.	40

FIGURE 3.3: Comparison of the corrected and uncorrected FRF for a CCCF rib.	41
FIGURE 3.4: Measured first mode shape, ψ_1 , with a natural frequency of 5757.9 Hz for the cantilever boundary condition.	42
FIGURE 3.5: Measured second mode shape, ψ_2 , with a natural frequency of 6319.4 Hz for the cantilever boundary condition.	43
FIGURE 3.6: Measured third mode shape, ψ_3 , with a natural frequency of 7939.1 Hz for the cantilever boundary condition.	43
FIGURE 3.7: Measured first mode shape, ψ_1 , with a natural frequency of 5994.4 Hz for the CCCF boundary condition.	44
FIGURE 3.8: Measured second mode shape, ψ_2 , with a natural frequency of 7795.7 Hz for the CCCF boundary condition.	44
FIGURE 3.9: Comparison of the predicted and measured direct FRF for CCCF boundary condition at an offset of 45 mm from the center of the free edge.	45
FIGURE 3.10: Comparison of the predicted and measured first mode stiffness at the free edge for the plate with CCCF boundary condition.	46
FIGURE 3.11: Comparison of the predicted and measured first mode stiffness at the free edge for the plate with cantilever boundary condition.	47
FIGURE 3.12: Dimensions for additional CCCF test geometries.	47
FIGURE 4.1: The resulting plot displays the aspect ratio (red circle) and curve fitting (blue line) for the cantilever plate.	55
FIGURE 4.2: The resulting plot displays the aspect ratio (red circle) and curve fitting (blue line) for the CCCF plate.	56
FIGURE 4.3: The plot displays the natural frequency values for a 72 mm tall CCCF plate.	57
FIGURE 4.4: The plot displays the natural frequency values for a 7.5 mm thick and 72 mm tall CCCF plate.	58
FIGURE 4.5: The plot displays the minimum stiffness values for a 72 mm high CCCF plate.	58
FIGURE 4.6: The plot displays the stiffness values for a 7.5 mm thick and 72 mm tall CCCF plate.	59

CHAPTER 1: INTRODUCTION

1.1 Thin-wall Machining

In the aerospace industry, high-speed milling of flexible components is a common manufacturing process. Features with wall thickness equal to sheet metal or even thinner are machined to produce monolithic components that mimic sheet metal build-ups. However, it is difficult to maintain dimensional accuracy and surface finish due to the relative displacement (vibration) between the thin wall and tool. Chatter is a common obstacle because the thin workpiece is flexible. Pioneering research by Smith and Tlustý [1-4] established processes which provide minimized cost, vibration, and chatter for successful thin-wall milling. They developed new NC programming routines to avoid cornering problems and optimal metal removal rate through permissible tool paths. Smith recognized that the two elements: optimal spindle speed, which corresponds most stable zone in the stability lobe diagram, and the limit of stability are related to tool length and workpiece flexibility and strongly affect the metal removal rate in high-speed milling [3, 4]. This, in turn, enabled selection of the tool length to match the stable zone to the highest spindle speed for highest metal removal rates. However, additional challenges arise when producing tall thin ribs. As the ribs are machined, many passes would be stable and produce acceptable surfaces. Then, during a particular pass, chatter would develop, damaging the previously machined surface.

According to Smith, as the machining progresses, the wall becomes more flexible. This is because, as the stable machining progresses, a certain rib height is reached where the part flexibility is low enough that the chatter-free depth of cut is exceeded. In order to eliminate the contact between the tool and the rib, relieving the tool (reducing the diameter) above the nominal cutting zone seemed a clever solution is shown in Figure 1.1. This principle of tool relief prevents the tool and rib contact during the forced vibrations of the rib.

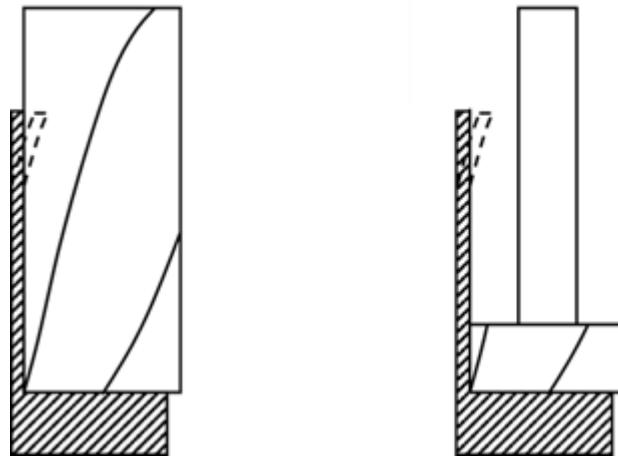


Figure 1.1: Machining of a thin-wall workpiece with conventional tool (left) and relieved tool (right) [4].

1.2 Literature Review

Thin-walled workpieces deform during cutting because of their low stiffness [5]. There has been a significant number of experimental, numerical, and analytical studies to make machining insensitive to the thickness. The following paragraphs summarize the relevant research and findings.

Thusty [6] and Tobias [7] studied machining vibrations; others continued their work [8-22]. Thusty [8] applied the orthogonal model to milling process by assuming the teeth

of the tool had equal pitch, were simultaneously in cut, and that the motion was rectilinear with constant depth of cut. The Nyquist criterion was used by Minis and Yanushevsky [9, 10] to identify the stability limit. Lee et al. [11, 12] used the mean value method to replace the time-varying directional coefficients by a constant. Altintas and Budak [13] proposed an analytical approach in which the average value in the Fourier series expansion of the time-varying coefficient was adopted. This analytical approach has been used to predict stable cutting conditions in milling [14-17]. Budak and Altintas [18, 19] showed that the results obtained by including the harmonic terms are very close to the single frequency solution. Campa et al. [20] applied the mono-frequency solution when considering the milling of thin walls and thin floors. They introduced the averaging of the cutting coefficients and the axial immersion angle along the cutting edge.

In the special case of thin-wall milling, a single stability lobe diagram cannot be applied directly because the dynamics change with the tool position and material removed. Thevenot et al. [21] studied the influence of material removal on dynamic behavior of the part by modeling it with constant dynamic properties and rigid body motion. The stability lobe change during machining was included as a third dimension on the stability lobe [22, 23]. This method was also extended by taking into account machine and tool flexibility [14]. Milling of workpieces with low rigidity, like thin walls requires that the static and dynamic effects and their evolution during machining be considered [24].

1.3 Research Objective and Scope

The objective of this study is to enable precision machining of thin features in hard-to-machine materials at high efficiency and low cost. A number of different alternative test geometries were evaluated for their performance in order to achieve this objective. Finite

element analysis was used to estimate structural stiffness for each test geometry and to evaluate the ability of each to support the anticipated machining forces. Figures 1.2 and 1.3 show first and second mode stiffness for different boundary conditions applied to an aluminum rib with a span length of 75 mm, a height of 20 mm, and a thickness of 3 mm thick. The stiffness was calculated as the ratio of applied force and the structure's displacement. The applied force was moved along the free edge of the wall to find the stiffness for each test geometry. For each of the test geometries from 1-10, symmetric geometry resulted in nodes. Qualitatively, for test geometry 7, the stiffness at these nodes is higher than the stiffness at the stiffeners. This study focuses on ribs that can be represented by clamped-clamped-clamped-free (CCCF) boundary condition. This boundary condition mimics thin ribs with lateral supports, or stiffeners, along their length. However, the cantilever boundary condition is also considered.

An analytical model is developed for the minimum lateral stiffness of thin ribs with CCCF boundary conditions. To identify the analytical model, the dynamic characteristics of the ribs are predicted using finite element analysis (ABAQUS/Standard 6.13) and multiple results from a broad range of rib dimensions are curve fit. The finite element (FE) accuracy is experimentally validated. The thin plate analysis is divided into two cases:

- Case I: cantilever boundary condition
- Case II: CCCF boundary condition

1.3.1 Case I: Thin-wall with Cantilever Boundary Condition

Altintas et al. [25] presented a dynamic model for peripheral milling of a flexible cantilever plate and rigid end mill by neglecting the time varying structural properties and the changes in the immersion boundaries. Budak and Altintas [26] considered the

peripheral milling of a flexible cantilever plate with slender end mills that incorporated the mechanistic force model and FE methods.

1.3.2 Case II: Thin-wall with CCCF Boundary Condition

Kline et al. [27] considered milling of a clamped-clamped-clamped-free (CCCF) plate with a flexible end mill. They used the FE method to model the plate and beam theory end mill. In order to enable precision machining of thin components, sacrificial structure preforms can be used to support the part during machining as described by Smith et al.[28].

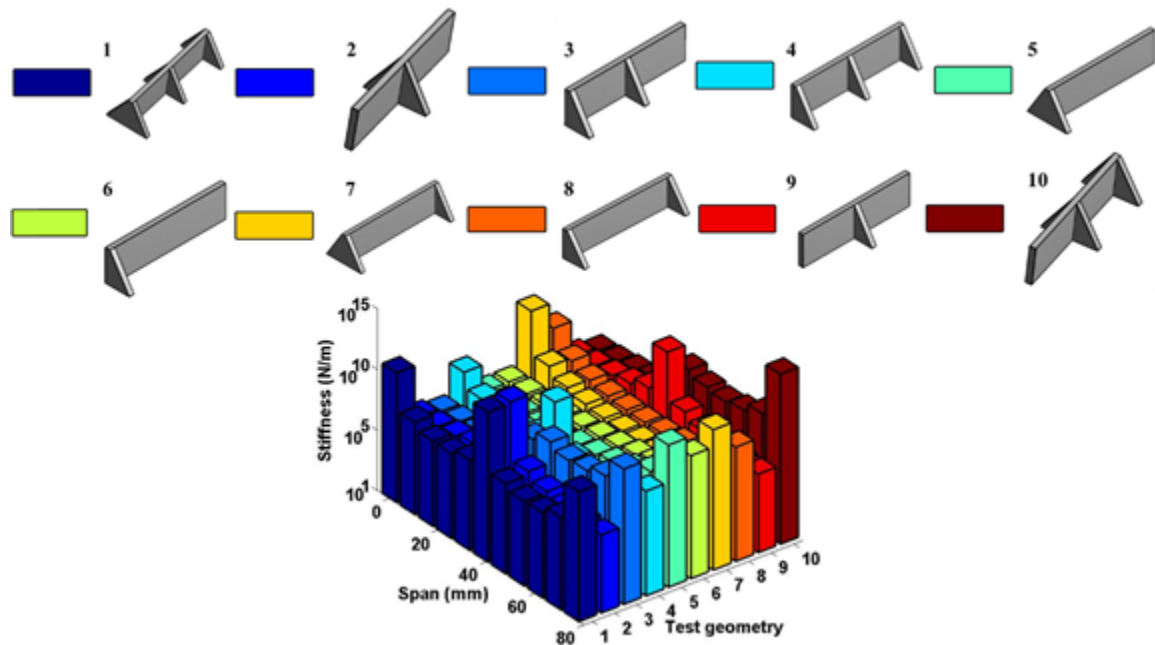


Figure 1.2: Predicted first mode stiffness for different boundary conditions.

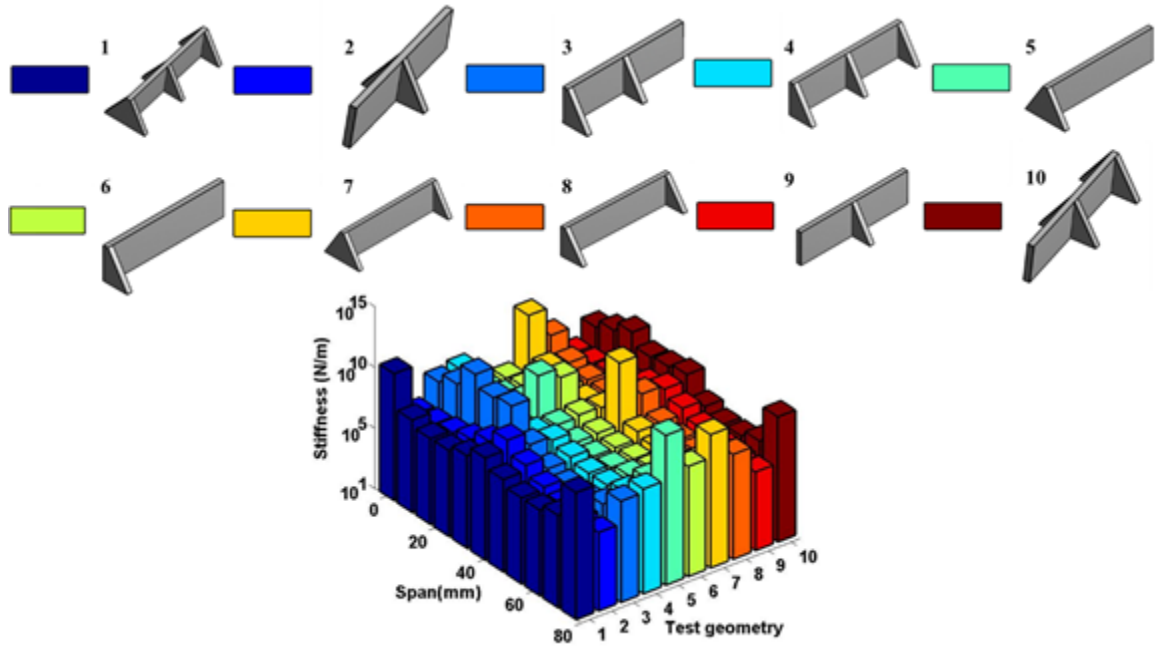


Figure 1.3: Predicted second mode stiffness for different boundary conditions.

CHAPTER 2: FINITE ELEMENT MODELING

2.1 Background

Numerical analysis is often selected to model complex structures, where analytical techniques may require excessive simplifications. The finite element method (FEM) is the most widely used numerical technique for structural analyses. In FEM, the continuum, or domain, is divided into a finite number of regions, called finite elements, which neither overlap nor have a gap between each other. The behavior of each element is controlled by the number of key points on each element called nodes. These nodes enable a problem with an infinite number of degree of freedom to be converted to one with a finite number using the differential equations of motion at each node. The motion of a dynamic structure or system may be represented by a set of simultaneous differential (coupled) equations using FEM. These coupled equations of motion are solved by transforming them into a set of independent (uncoupled) equations by means of a modal matrix (composed of the system eigenvectors). This procedure is called numerical modal analysis [29]. Modal analysis is a process for determining the system's modal parameters, including natural frequencies (eigenvalues) and mode shapes (eigenvectors). Finite element analysis offers an effective predictive capability for modelling the thin-walled structures considered in this study.

2.2 ABAQUS/Standard Overview

ABAQUS/Standard is an analysis tool that provides solutions for structural, thermal, modal, and shape optimization studies. It reduces the need for multiple prototypes and

product testing by effectively verifying the product performance and reliability from the concept phase through the various product design and development stages.

The software includes preprocessing, simulation, and postprocessing, which are three distinct stages linked together as shown in Figure 2.1.

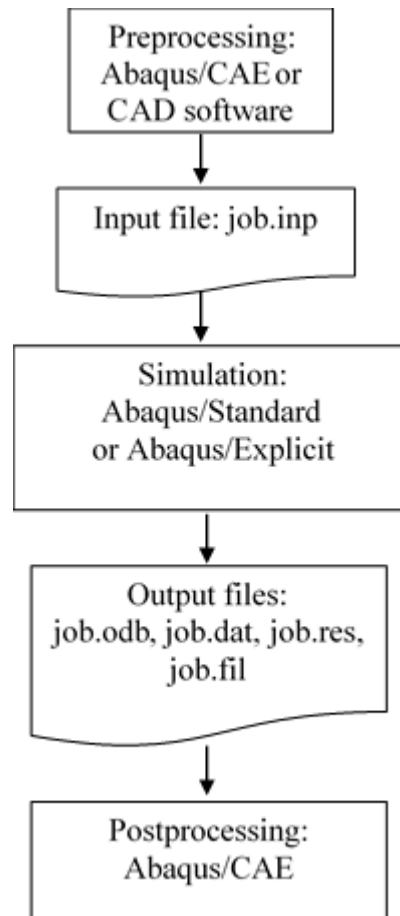


Figure 2.1: ABAQUS analysis stages.

2.2.1 Preprocessing

This is a part modelling stage where a model is created using ABAQUS/CAE (Computer Aided Engineering) or imported from a computer aided drawing (CAD) software such as Solidworks. The complete model definition includes material properties, boundary conditions, and forces. The basic information regarding the model, from the geometry to the applied loads, is stored in an input (.inp) file.

2.2.2 Simulation

In the simulation stage, ABAQUS/Standard or ABAQUS/Explicit solves the numerical problem defined in the model.

2.2.3 Postprocessing

After successfully completing the simulation stage, ABAQUS generates an output database file (.odb). This file contains the simulated results, such as the deformed shapes, colored contour plots, and animations, which can be viewed using the ABAQUS/CAE Visualization module.

2.2.4 Analysis Procedure

In ABAQUS/Standard, modal analysis is referred to as dynamic analysis, where the response of linear systems are calculated based on the mode shapes and natural frequencies. The procedure for dynamic analysis is summarized in the following sections.

2.2.4.1 Natural frequency extraction

Eigenvalue extraction is used to calculate the natural frequencies and the corresponding mode shapes of a system using the Lanczos eigensolver. The eigenvalue problem for natural frequencies of an undamped finite element model is given by Eq. (2.1),

$$(-\omega^2 M^{MN} + K^{MN}) \phi^N = 0, \quad (2.1)$$

where M^{MN} is the symmetric and positive definite mass matrix; K^{MN} is the stiffness matrix; ϕ^N is the eigenvector; and M and N are the degrees of freedom [30].

The following steps are completed in the natural frequency extraction:

When ABAQUS/CAE begins, the *Start Session* dialog appears which is shown in Figure 2.2.

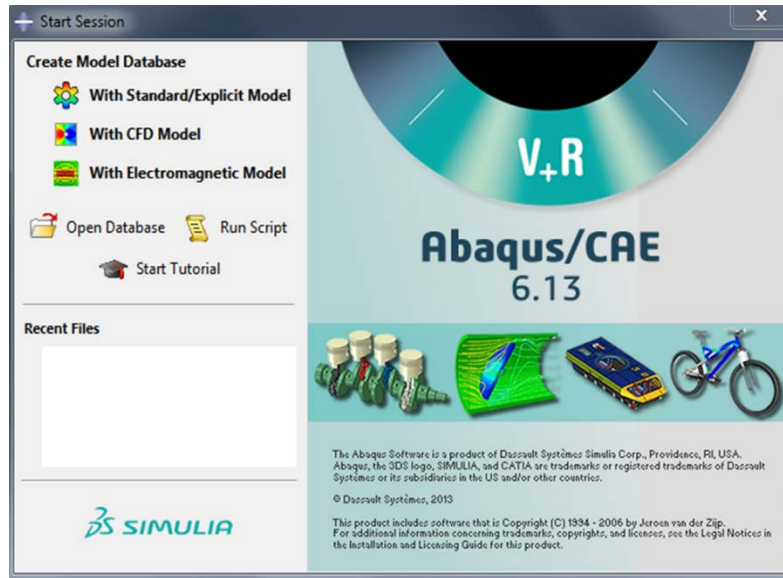


Figure 2.2: The *Start Session* dialog box.

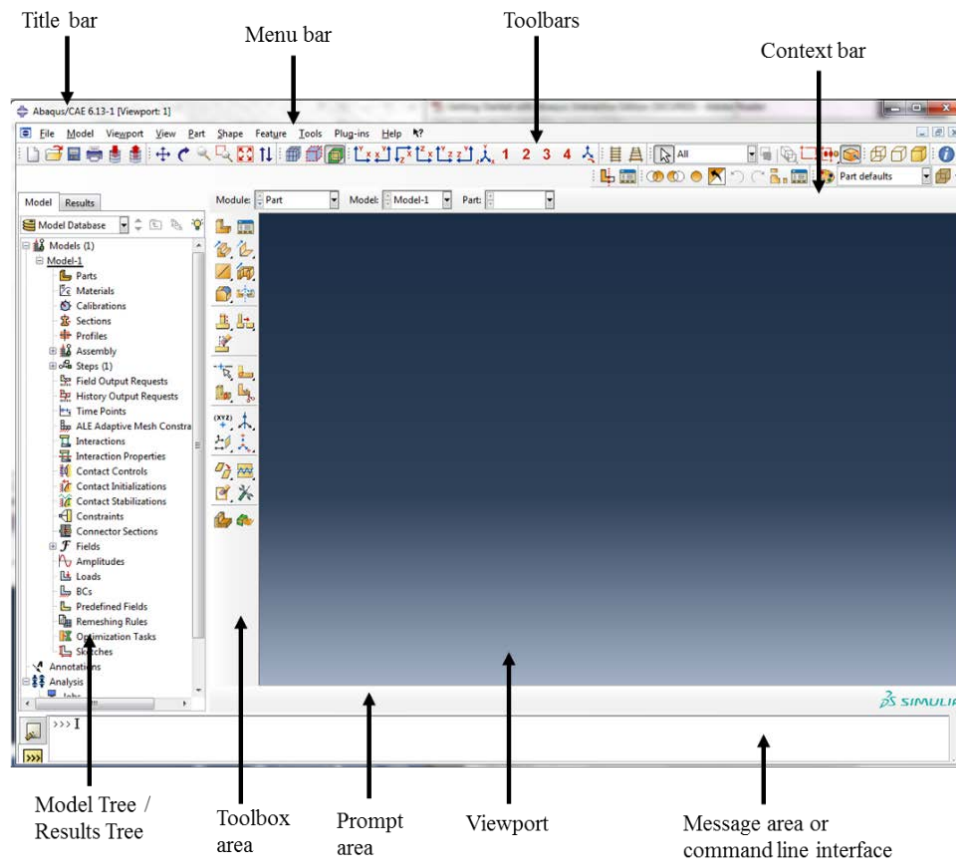



Figure 2.3: Components of the main window.

For modal analysis, select *Create Model Database – With Standard/Explicit Model*. This enables a new ABAQUS/Standard or ABAQUS/Explicit analysis to be started. The main window along with its components, as shown in Figure 2.3, will appear. For detailed information, refer to ABAQUS/CAE User’s guide “Components of main window” section 2.2.1 [30].

Step-I: Creating a part

By default, ABAQUS/CAE starts the main window in the Part module. The part module provides a set of tools that allows the user to add and modify the features that define a part. Before making any modification in the ABAQUS/CAE, select *File menu* and *Set Work Directory* and then choose a specific directory to save the CAD and result files.

Create a part using the  tool in the *Part module* toolbox. In the Create Part dialog box, see Figure 2.4, type a name for the part in the *Name* text box.

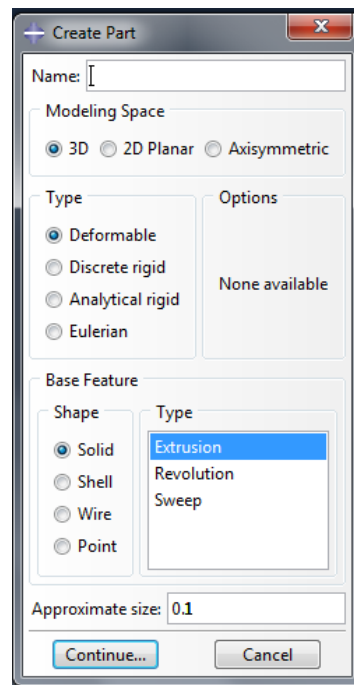


Figure 2.4: The *Create Part* dialog box.

- For *Modeling Space*, select *3D*, which creates a three-dimensional (3D) part
- For *Type*, select *Deformable*, which creates a part that can deform under load
- *Base Feature*
 - For *Shape*, select *Solid*
 - For *Type*, select *Extrusion*
- For *Approximate size*, type 0.1. This is used to calculate the size of the Sketcher sheet and the grid spacing. The approximate size should be equal to or greater than the largest dimension of the part. See Figure 2.5.

ABAQUS/CAE does not use specific units, but the units must be consistent throughout the model. In this research, the length unit is meters.

Using the data provided in Figure 2.6, the top right section is used to create a 3D model of a thin-walled structure with a cantilever boundary condition.

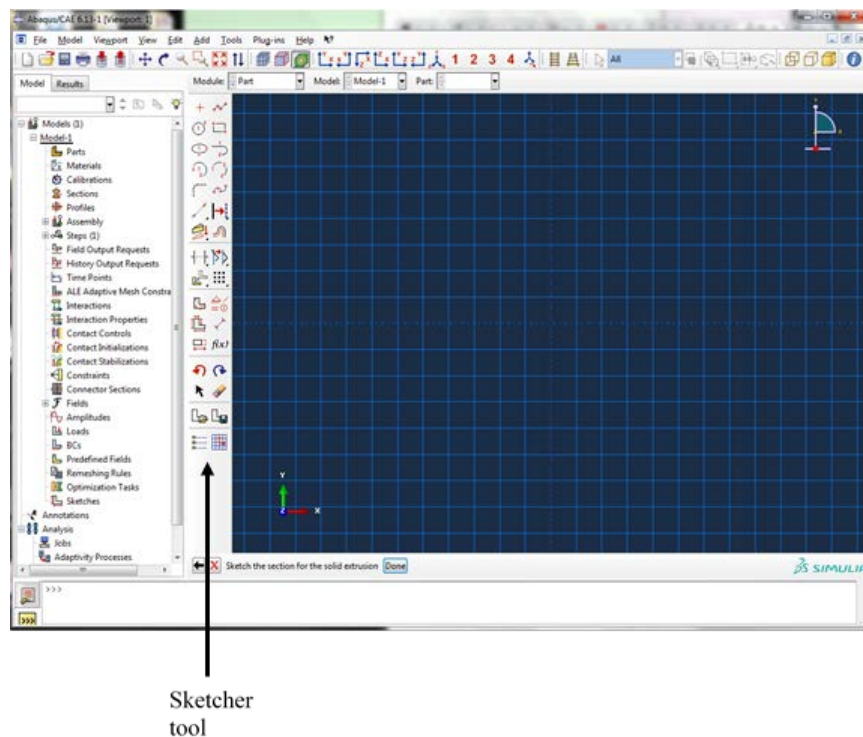


Figure 2.5: The Sketcher grid with a grid size of 0.1.

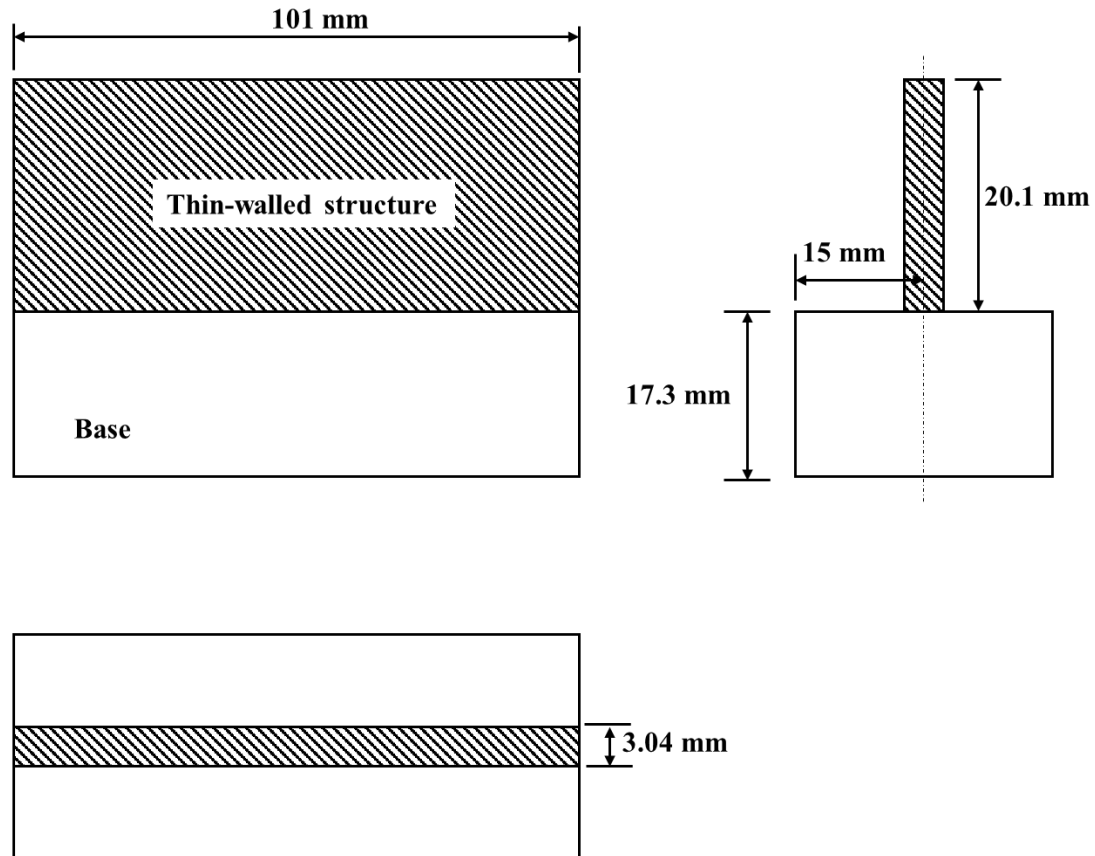








Figure 2.6: Two-dimensional (2D) detailed drawing of an aluminum Al-6061 thin-walled structure with cantilever boundary condition.

To draw the 2D sketch for the base, select  *Create Construction: Oblique line through two points* tool to create horizontal and vertical center lines on the Sketcher grid as shown in the Figure 2.7. Sketch in the X-Y plane and press the scroll button on the mouse to exit the selected command. The horizontal and vertical constraints on the center line are denoted by *H* and *V*. Then select  *Create Lines: Rectangle (4 points)* tool to create the base as shown in Figure 2.8. When sketching the base, make the base symmetric in the vertical and horizontal axis by selecting  *Add Constraint* tool from the Sketch tool and select *Symmetry*. This defines the symmetry constraint for the part from the *Constraints* dialog box. To make the base sketch symmetric about the vertical axis, select the vertical

center line as the *axis of symmetry* and select the line to left of the vertical center line as the *first entity for symmetry constraint* and right as the *second entity for symmetry constraint*. To constrain the base with respect to the center lines, select *Fixed* from the *Constraints* dialog box and select both the center line using shift key and press *Done* as shown in Figure 2.9. To assign the dimensions, select  *Add Dimension* tool and select the horizontal and vertical edges to be 0.0153 and 0.0173 as shown in Figure 2.10.

To sketch the thin-wall feature sketch, select  *Create Lines: Rectangle (4 points)* tool and create a rectangle as shown in Figure 2.11. Constrain the sketch using the *Symmetry*, *Fixed*, and *Coincident* constraints to make sure the base of the thin-wall feature sketch coincide with the base feature sketch using *Add Constraint* in the *Sketcher Tool*. Dimension the sketch with horizontal and vertical edges to be 0.02 and 0.0015 as shown in Figure 2.12. Figure 2.13 shows self-intersecting lines in the sketch which can be removed using  *Auto-Trim* tool and then the *Horizontal* constraint to constrain the top part of the base feature sketch because the trim operation un-constrains the feature. The fully constrained base and thin-wall feature sketch is shown in Figure 2.14.

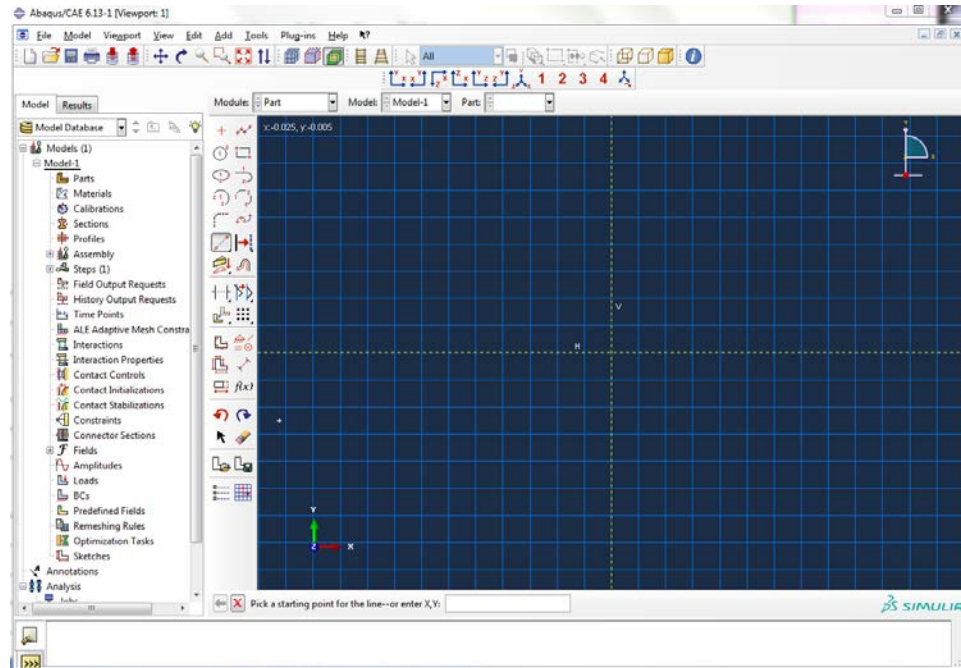


Figure 2.7: Sketching the horizontal and vertical center line on the Sketcher grid.

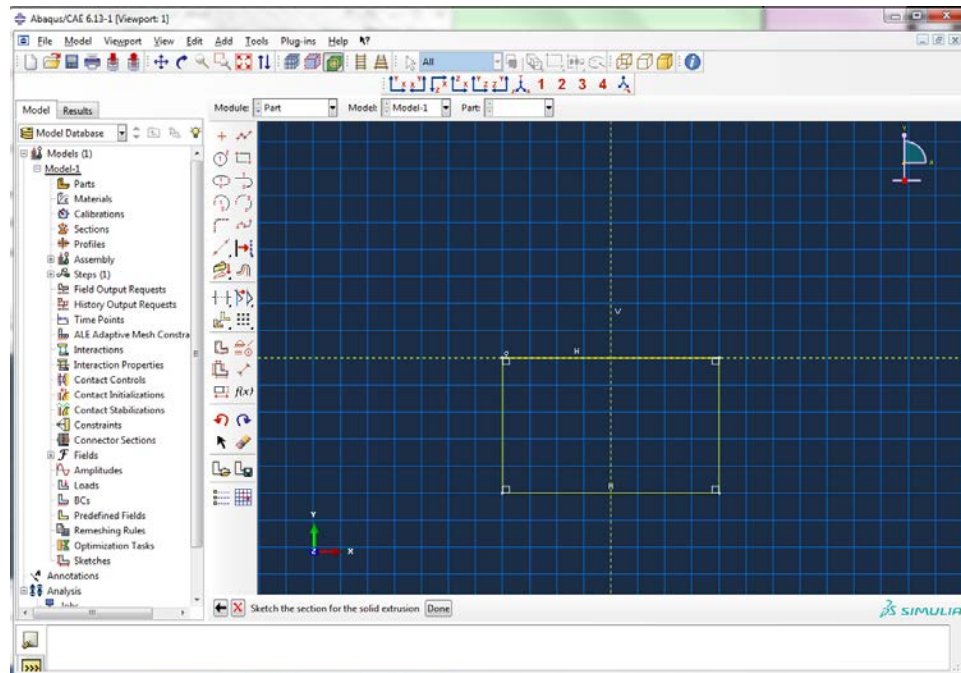


Figure 2.8: Sketching the base feature.

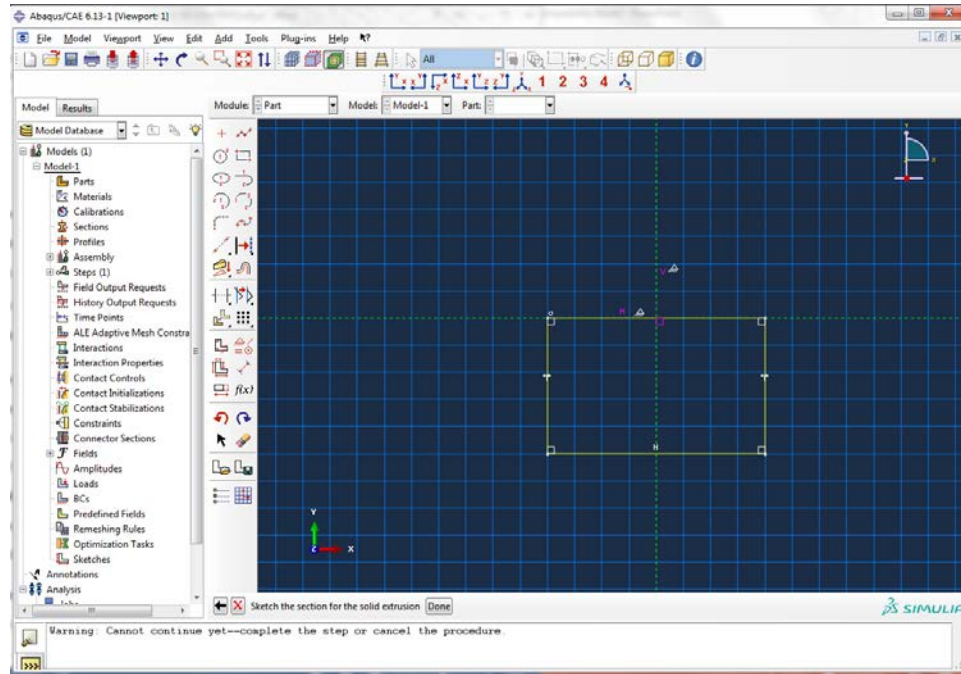


Figure 2.9: Sketching the constraints.

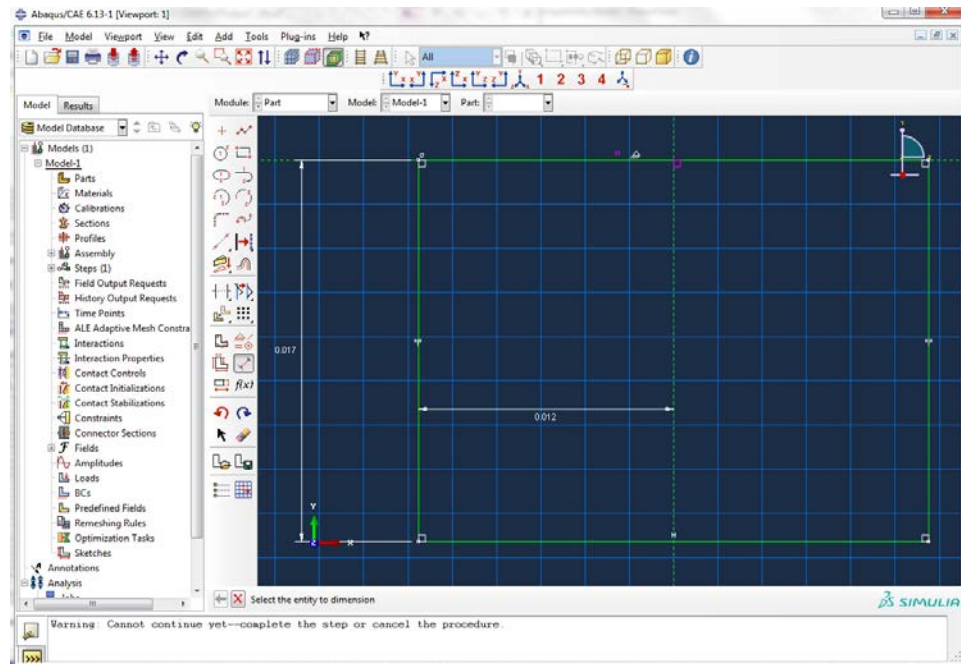


Figure 2.10: Base feature sketch with all dimensions and constraints.

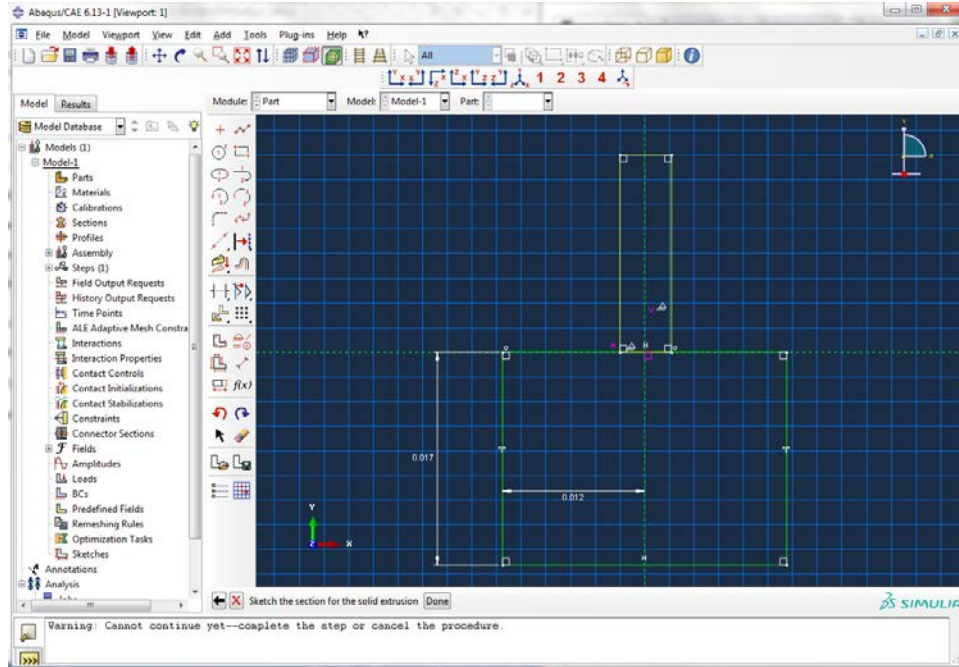


Figure 2.11: Sketching the thin-wall feature.

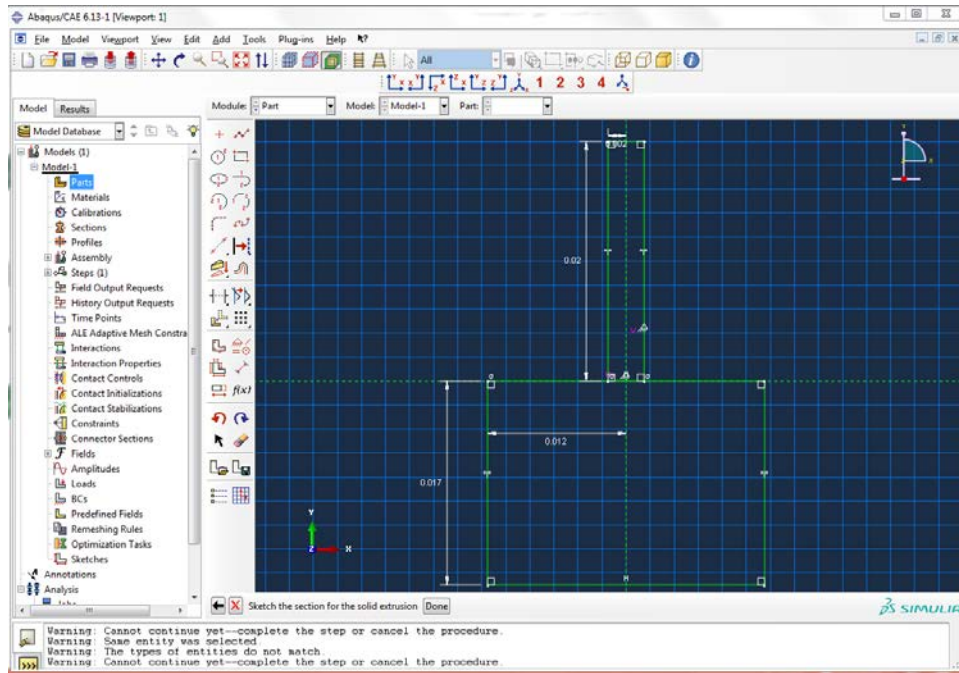


Figure 2.12: Base and thin-wall feature sketch with all dimensions and constraints

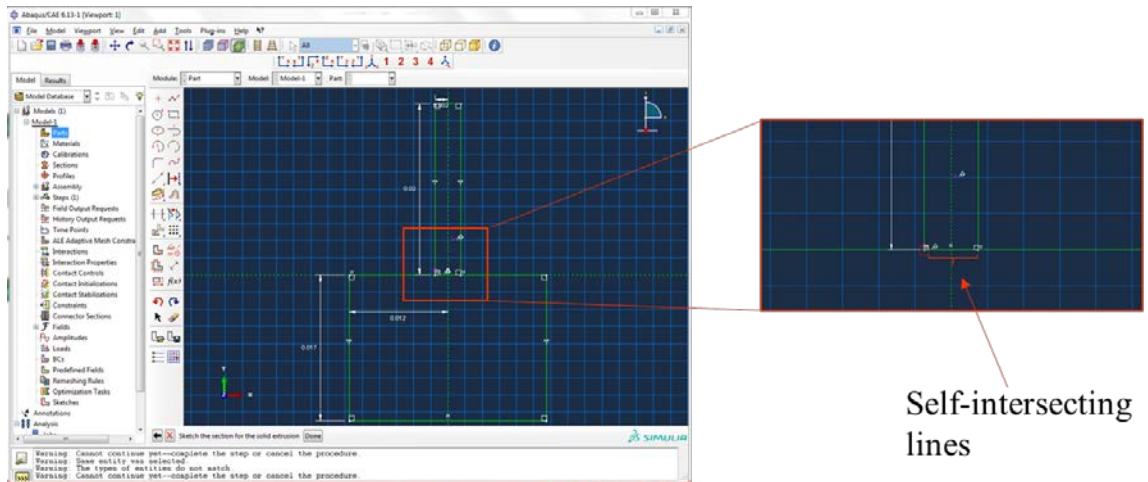


Figure 2.13: The self-intersection zone between the base and thin-wall feature sketch.

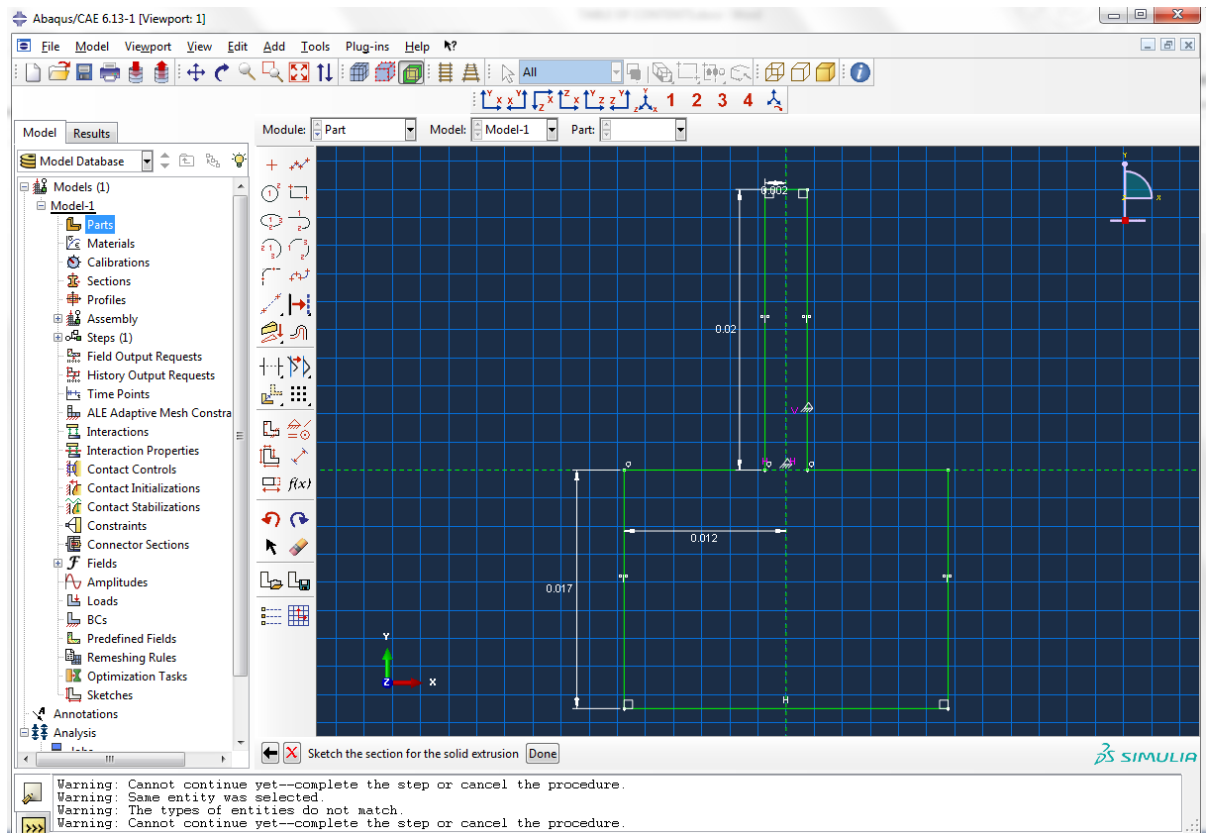


Figure 2.14: Fully constrained sketch for the base and thin-wall feature.

After defining a fully constrained base thin-wall feature sketch press *Done* to switch back from the Sketching grid to modeling and enter 0.01, the desired length, in the *Depth* text box, which is available in the *Edit Base Extrusion* dialog box. Press *OK* to generate a

3D solid CAD model for a thin-wall structure with cantilever boundary condition as shown in Figure 2.15.

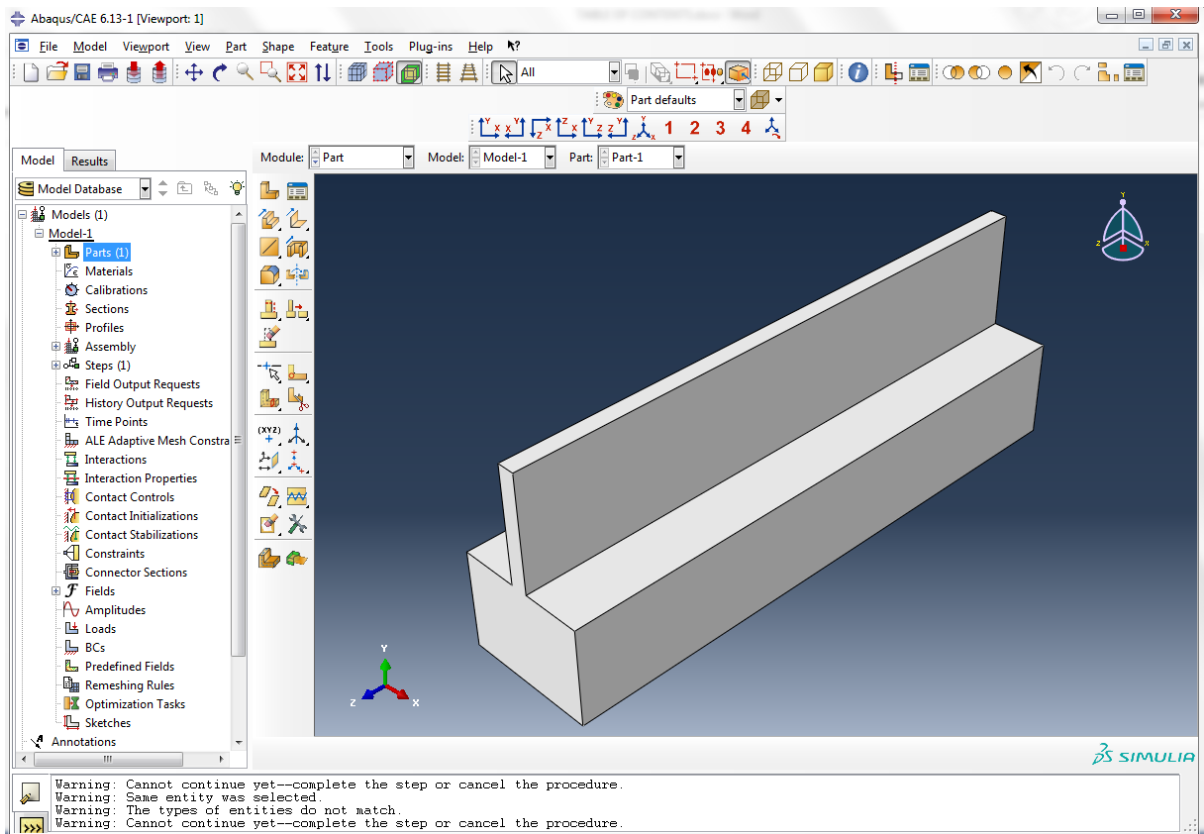
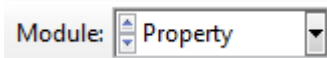
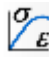


Figure 2.15: Extruded solid 3D CAD model for a thin-wall structure with cantilever boundary condition.

Step-II: Assign material properties

The 3D CAD model for a thin-wall structure now needs the material properties to be

assigned. This is performed in the *Property module*. Select  in

the *Module* drop down box. In the *Toolbox area* select the  *Create Material* tool which will display the *Edit Material* dialog box as shown in Figure 2.16 and enter the following information.

- *Name*: Aluminum-6061
- select *General* → *Density*; *Mass Density*: 2700

- select *Mechanical* → *Elasticity* → *Elastic*;
 - *Young's Modulus*: 68.9e9
 - *Poisson's Ratio*: 0.33

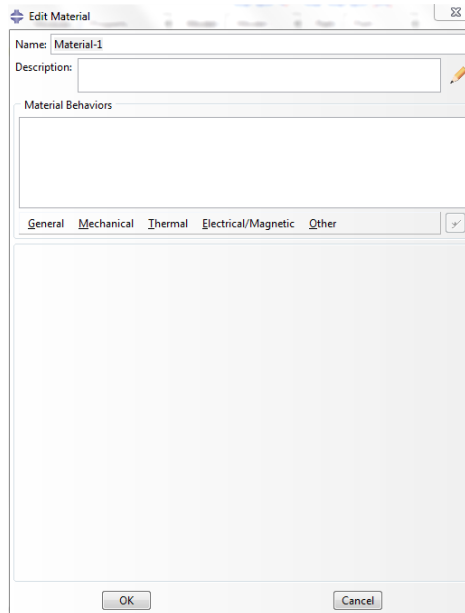



Figure 2.16: *Edit Material* dialog box.

A cross-section should be defined for a part and this cross-section is assigned to each instance of the part. To assign a section select  *Create Section* in the *Create Section* dialog box and type the following information.


- *Name*: Thin_wall_structure
- *Category*: Solid
- *Type*: Homogeneous

A solid with homogeneous properties is assigned to the thin-wall 3D CAD model, which makes it similar to a monolithic thin-wall structure.

The *Edit Section* dialog box, which displays *Name* as *Thin_wall_structure*; *Type* as *Solid*, *Homogenous*, requires the user to assign a material to this section, *Thin_wall_structure*. In

the *Material* drop down box, select *Aluminum-6061* . The

section now has its material properties defined, but it is not yet assigned to the CAD model.

In order to do so, select  *Assign Section* and select anywhere on the surface of the CAD model and click *Done*. An *Edit Section Assignment* dialog box will display the data displayed in Figure 2.17, which indicates that the *Picked* region will be assigned with a section named *Thin_wall_structure* of solid, homogenous *Aluminum-6061* material properties; see Figure 2.18.

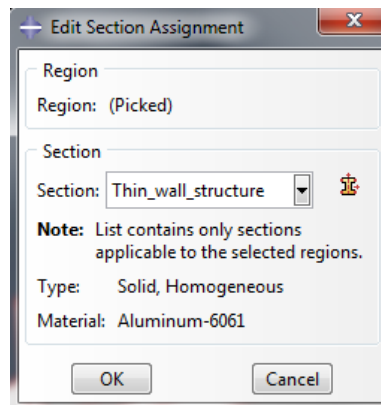


Figure 2.17: The *Edit Section Assignment* dialog box indicates that a section named *Thin_wall_structure* made of Aluminum-6061 will be assigned to the CAD model.

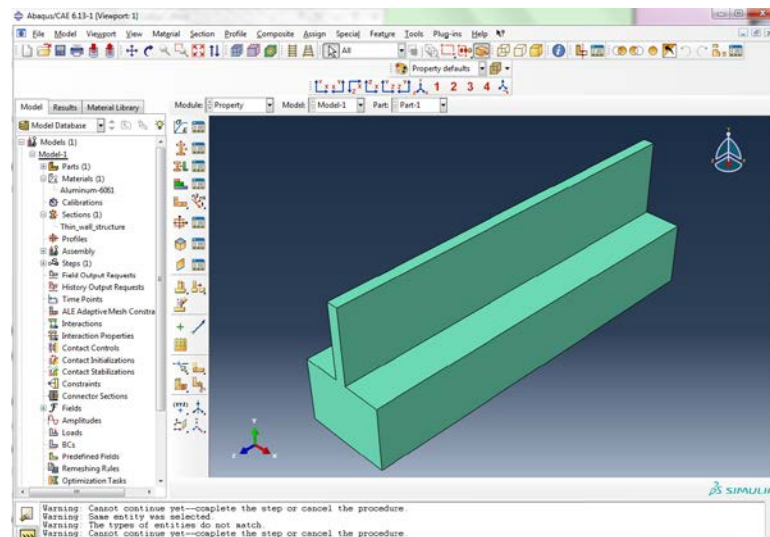



Figure 2.18: Al-6061 material properties assigned to thin-wall 3D CAD model.

Step-III: Assign global coordinate system

When a part is created in the *Part Module*, it is positioned relative to its local coordinate system. The instances of the part are created and these instances are positioned relative to global coordinate system, thus creating an assembly. To create a part or model

instance, select *Assembly* from the *Module* drop down box  and

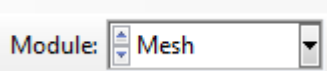
select  *Create Instance*. Select the following in the *Create Instance* dialog box:


- *Create instances from*: Select the part
- *Instance Type*: *Independent*


and press *OK*. *Dependent* type instance enables each part to be meshed first, rather than the entire assembly, and will not allow any part modification, in the *Assembly Module*. In contrast, the *Independent* instance type allows instance meshing (that is, the user can either mesh each part or the assembly) and allows part modification in the *Assembly Module*.

Step-IV: Create mesh

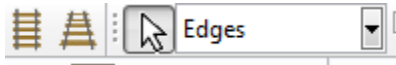
After successfully assigning global coordinates, the thin-wall model with cantilever boundary condition is meshed using the Mesh Module. Select *Mesh* from the *Module* drop

down box . By default, ABAQUS/CAE assigns the mesh seeds

and controls the mesh density on the part edge. Select  *Seed Edges* to preview the default mesh seeds on the part edges as shown in Figure 2.19. To preview the mesh quality

with respect to the default mesh seed select  *Mesh Part Instance* and press *Yes* to apply the mesh. The top-down mesh quality with respect to the default mesh seeds is not uniform as shown in Figure 2.20. This is due to the shape of the CAD model. To apply a uniform

mesh for the part instance, divide the part into simple regions, i.e., divide the thin-wall feature from the base feature, which is achieved using the *Partition* operation in the *Part Module*. Using the *Partition* operation on the part will not have any effect on the final result because the nodes of these divided features will be connected making it a monolithic feature. Select *Part* in the *Module* drop down box to switch to *Part Module* and select *Tools* from the *Menu bar* and *Partition. Create Partition* will appear on the screen; select *Cell* for *Type* and *Define cutting plane* for *Method*. In the prompt area it is required to *specify the plane* (that is, define the cutting plane); select *3 Point*. Note that the points should not be collinear. Select the three points at the intersection of the thin-wall and base feature and select *Create Partition* in the *Prompt area*. The edges of the top part of the base are now divided into three parts in the X-Y plane, select *Edges* in the *Tool bar*



and move the pointer on the top edges of the base feature to identify these three edges. There will be a change in the mesh density between the top and bottom edges in the X-Y plane of the base feature, so the base feature will be partitioned. Select the *base feature* for the *cells to partition* and *specify the plane* as *Point & Normal*. Select the point at the intersection in the X-Y plane and a line passing through the point in the same plane. Now the base is divided into two parts. Similarly, select the opposite cell/region and partition it *using Point & Normal* partition and this should now divide the base into three parts. To learn more about *Partition* operation refer to ABAQUS/CAE file [30]. To verify that the thin-wall and base feature are now a separate

cell or region select  *Cells* in the *Tool bar*. By dragging the

pointer on the part, it will indicate that the features are divided.

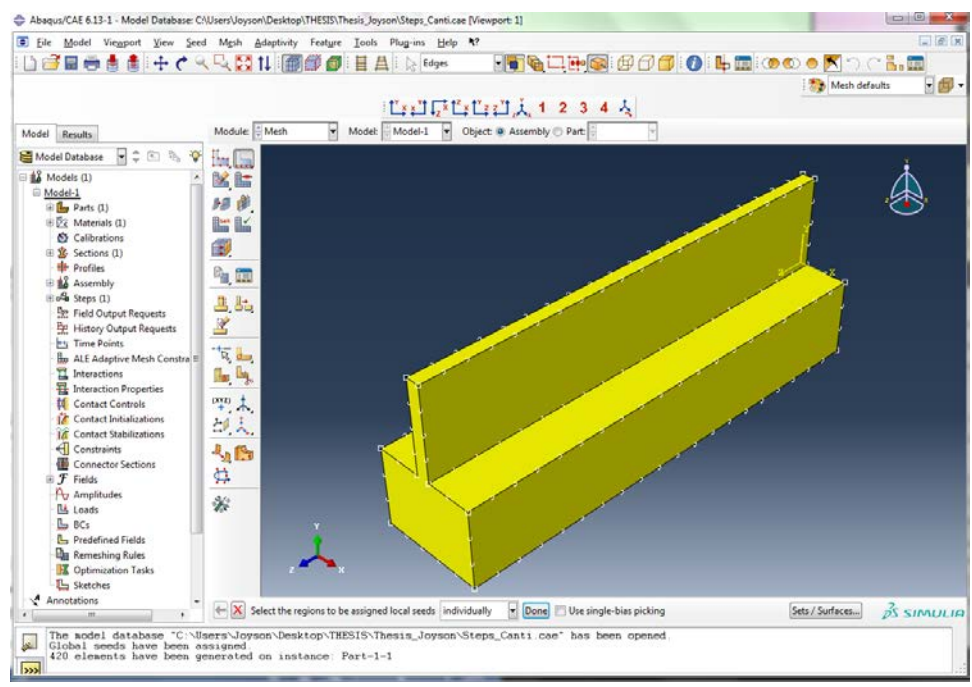


Figure 2.19: The thin-wall with cantilever boundary condition with default mesh seed in mesh module.

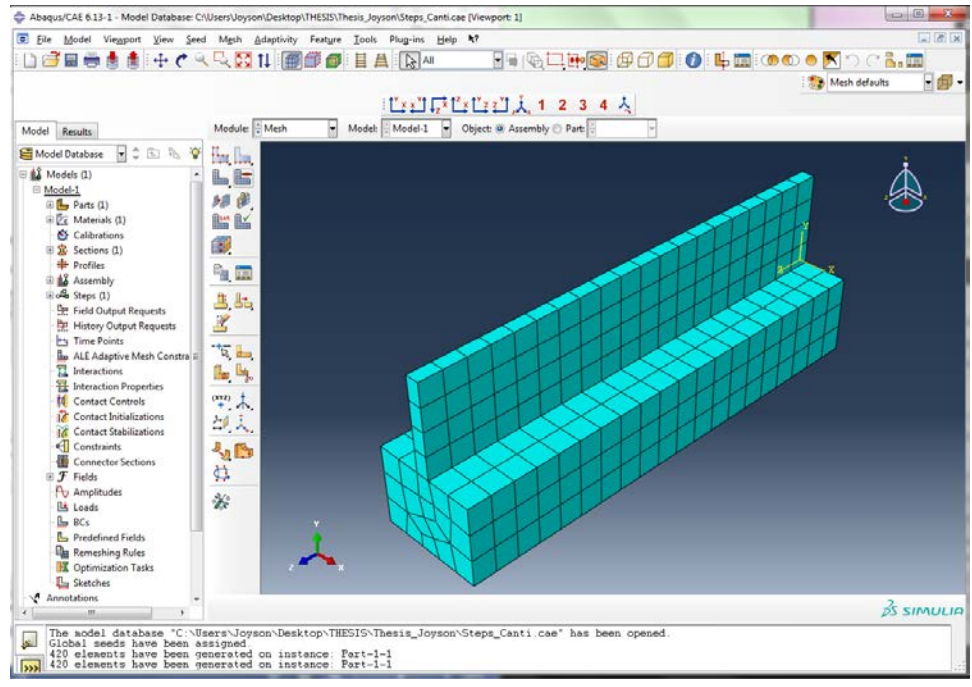



Figure 2.20: Poor mesh quality of the with respect to the default mesh seeds with 420 elements.

Now switch to *Mesh Module* and, because the part instance type is *Independent*, select

Object: **Assembly** *Assembly for Object*. Select  *Mesh Part Instance* to assign the mesh on the part which is shown in Figure 2.21. The mesh assigned to the part is linear hexahedral elements of type C3D8R (eight-node linear brick with reduced integration and hourglass control). Approximately, 91908 elements and 101024 nodes are found to be enough after convergence of the natural frequency and stiffness (mesh refinement studies are presented in Figure 2.22) to model the thin-wall structure with cantilever boundary condition.

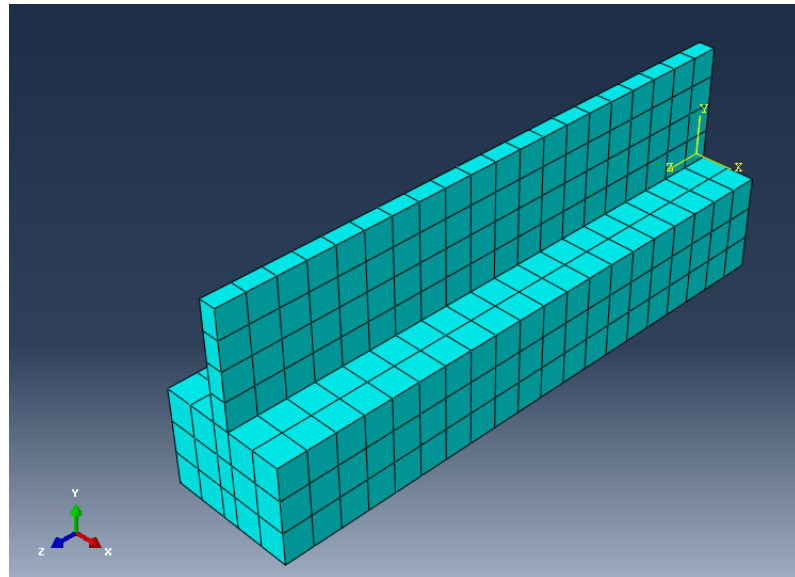


Figure 2.21: Uniform mesh quality throughout the part with 672 nodes and 380 elements.

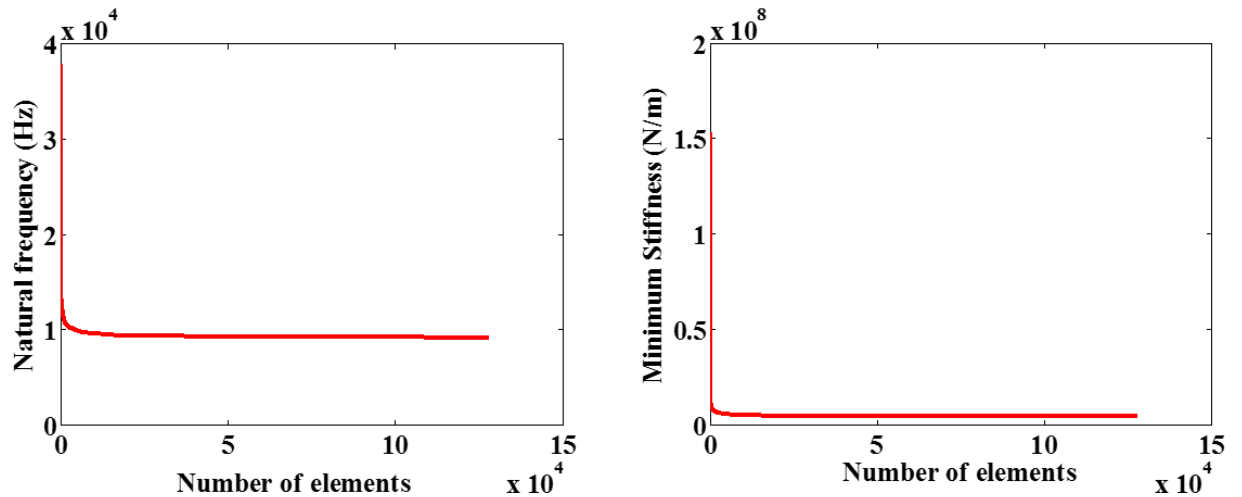


Figure 2.22: Effect of mesh refinement on natural frequency (left) and minimum stiffness (right).

Step-V: Boundary condition

For the experiments, the base of the thin-wall monolithic structure with cantilever boundary condition was fixed to a rigid table using cyanoacrylate. The ABAQUS/CAE model approximately applies the same boundary condition. To set the boundary condition,

select the analysis type (Natural Frequency Extraction). Select



Step from the *Module* drop down box then  *Create Step* so that a Create Step dialog box appears on screen and then enter the following data:

- *Name*: Natural Frequency Extraction
- *Procedure type*: *Linear perturbation*
- select *Frequency*

in the *Edit Step* dialog box and select *Lanczos Eigensolver* (default) and *Value* in the *Number of eigenvalues requested* and enter 3 (determines the natural frequency for the first three modes). After selecting the analysis type, ABAQUS/CAE allows the user to select the boundary condition for the analysis. Now switch to *Load* module

Module: and select  *Create Boundary Condition*. In the *Create Boundary Condition dialog* box, enter the following data.

- *Name*: Fixed
- *Step*: Natural Frequency Extraction
- *Procedure*: Frequency
- *Category*: Mechanical
- *Types for Selected Step*: *Symmetry/Antisymmetry/Encastre* (constraint on all displacements and rotations)

Press *Continue* and it will prompt the user to *Select the regions for boundary condition*.

Select the bottom face of the base (see Figure 2.23) and press *Done*. Select *ENCASTRE* in the *Edit Boundary Condition dialog* box.

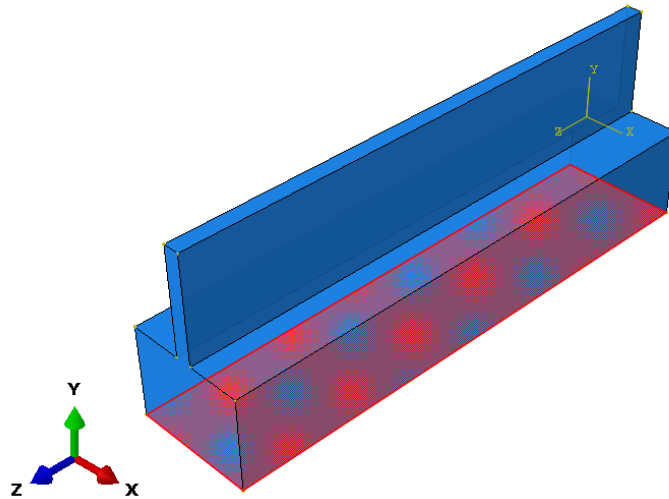
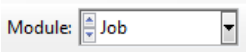



Figure 2.23: FEM encastre boundary condition: the bottom face is constrained from all displacements and rotations.

Step-VI: Run the analysis

To run the natural frequency extraction analysis, switch to  *Job* module, select  *Create Job*, and enter the desired name for the *Job* in the *Name* text box. Press *Continue*, which will open an *Edit Job dialog box*, and in the *Description* tab enter the description of the analysis (optional).

Step-VII: Results

Once the simulation is completed, a message will displayed in the Message area box. The results for the Natural Frequency Extraction analysis can be viewed by selecting the *Job* menu and *Results*. It will indicate the name of the job and the Viewport window as shown in Figure 2.24 will appear.

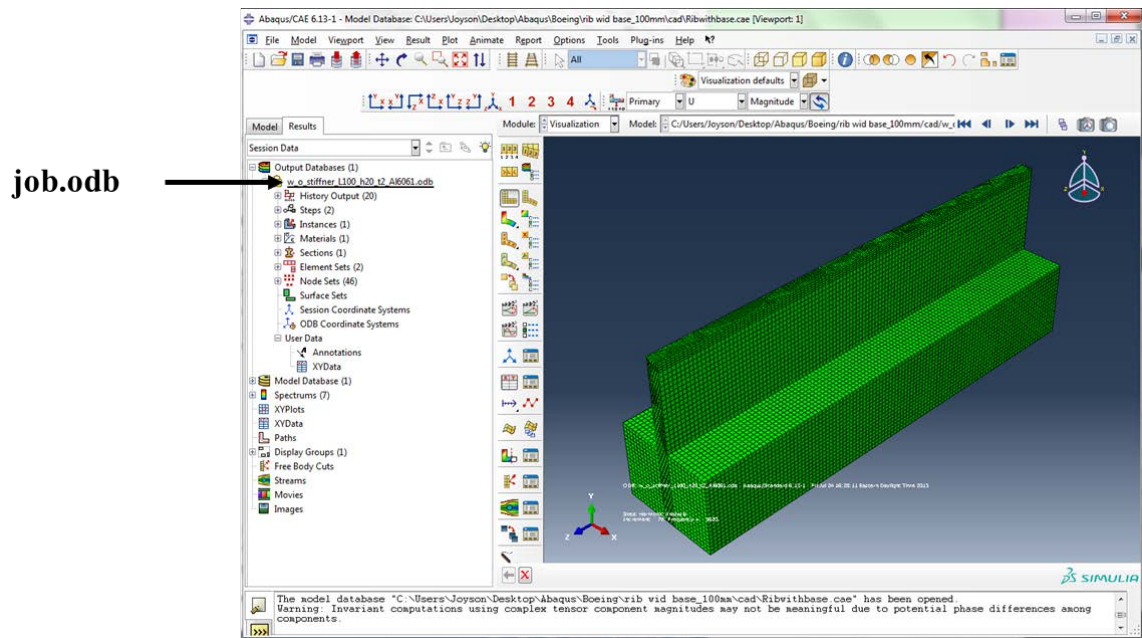



Figure 2.24: Viewport window displaying the undeformed shape of the thin-wall structure with cantilever boundary condition.

The mode shapes can be viewed by selecting  *Plot Contours on Deformed Shape* and changing the deformation scale by selecting the *Options* menu and *Common*, checking

Uniform, and entering 0.0001. By selecting *Step/Frame* from the *Result* in the menu bar, the *Step/Frame* dialog box will be displayed as shown in Figure 2.25.

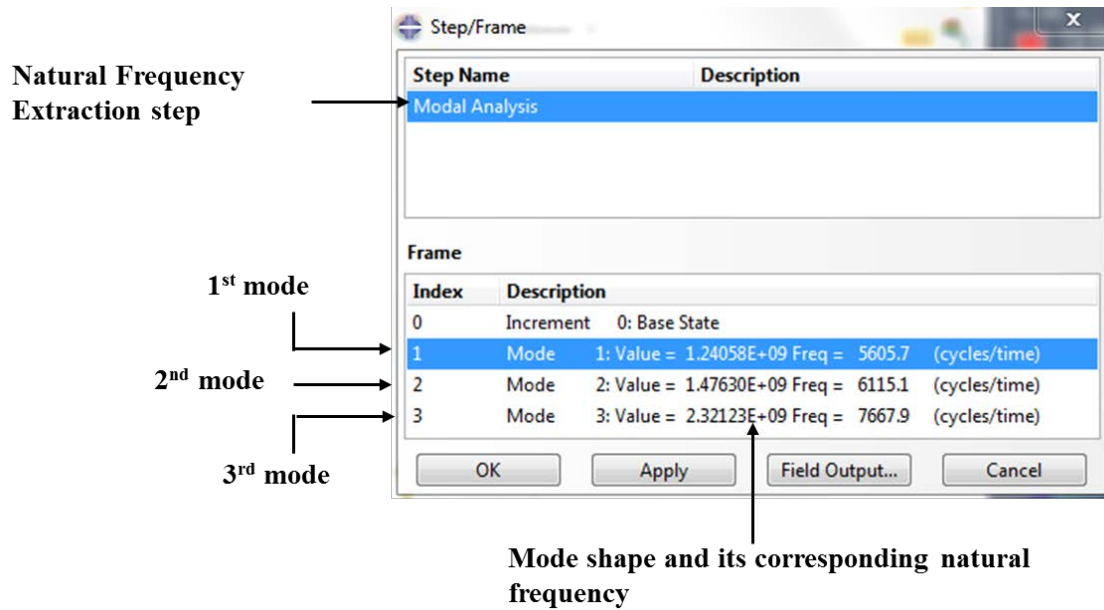


Figure 2.25: Step/Frame dialog box displaying the mode and its corresponding frequency for thin-walled structure with cantilever boundary condition.

Figures 2.26 to 2.28 shows the predicted mode shapes and corresponding natural frequencies for the cantilever boundary condition.

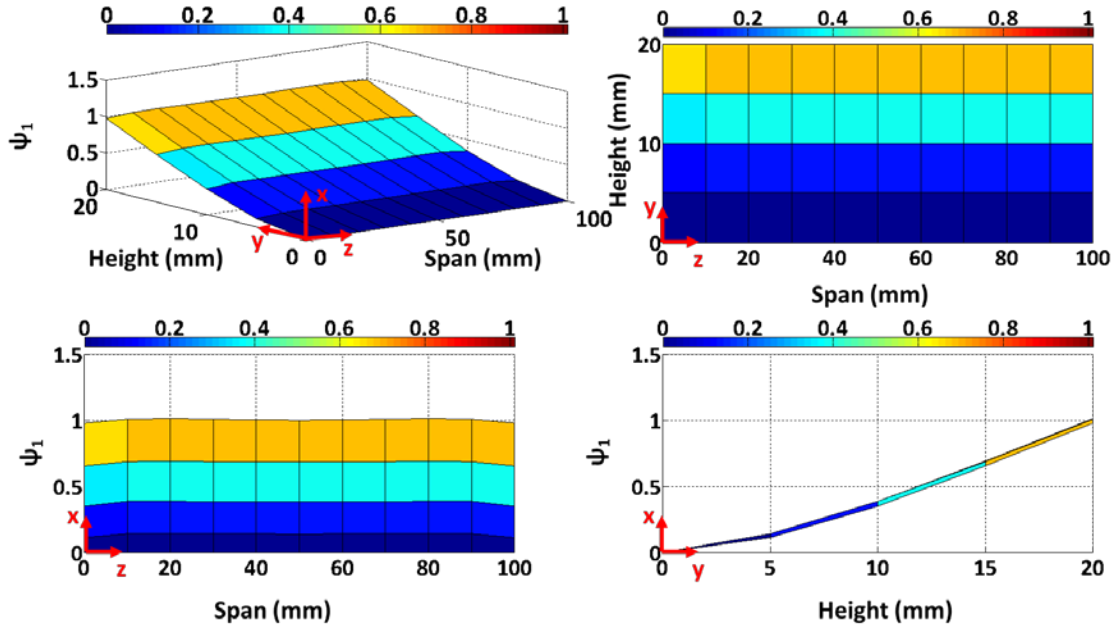


Figure 2.26: Predicted first mode shape, ψ_1 , with a natural frequency of 5605.2 Hz for the cantilever boundary condition.

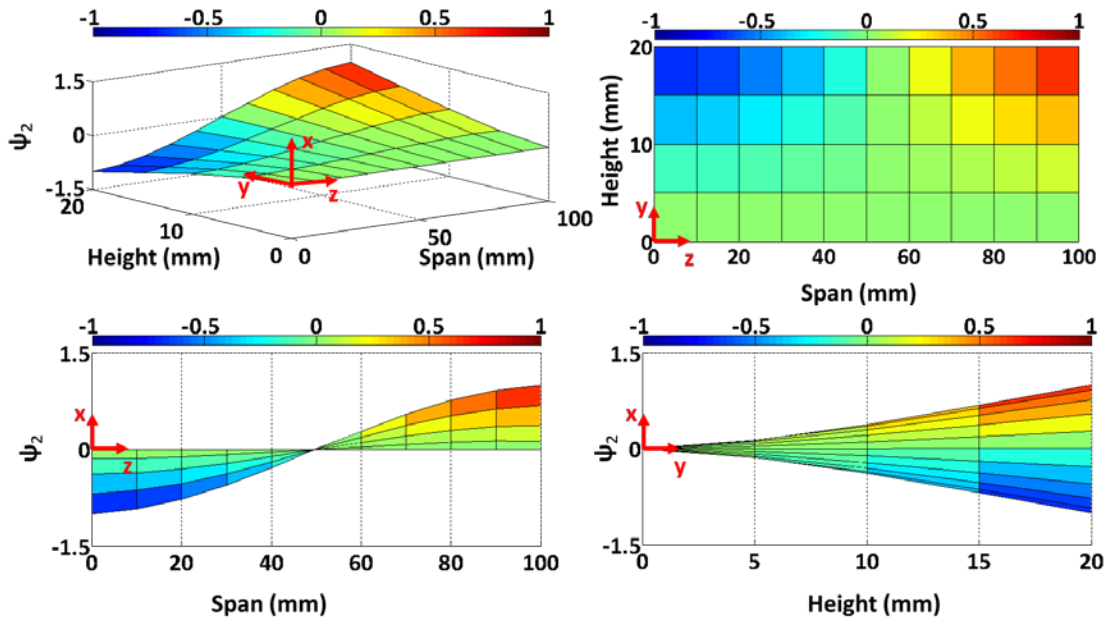


Figure 2.27: Predicted second mode shape, ψ_2 , with a natural frequency of 6115 Hz for the cantilever boundary condition.

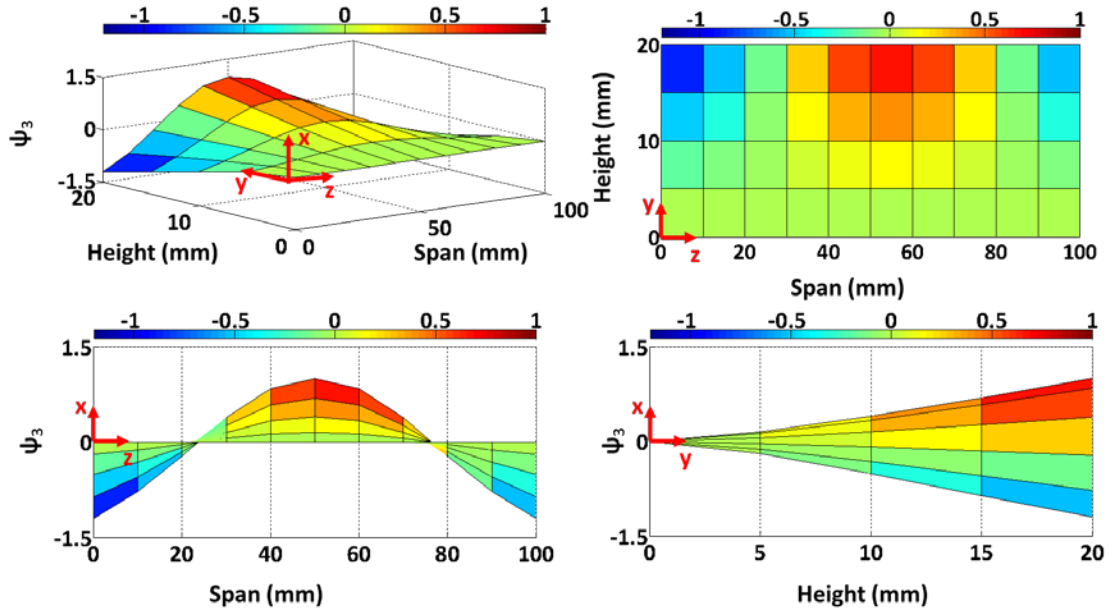


Figure 2.28: Predicted third mode shape, ψ_3 , with a natural frequency of 7668.5 Hz for the cantilever boundary condition.

Repeat the Steps I to VII to model the thin-walled structure with clamped-clamped-clamped-free (CCCF) boundary condition as shown in Figure 2.29. Here, 138306 nodes and 126456 elements were used to predict the mode shapes and corresponding natural frequencies; see Figures. 2.30 and 2.31.

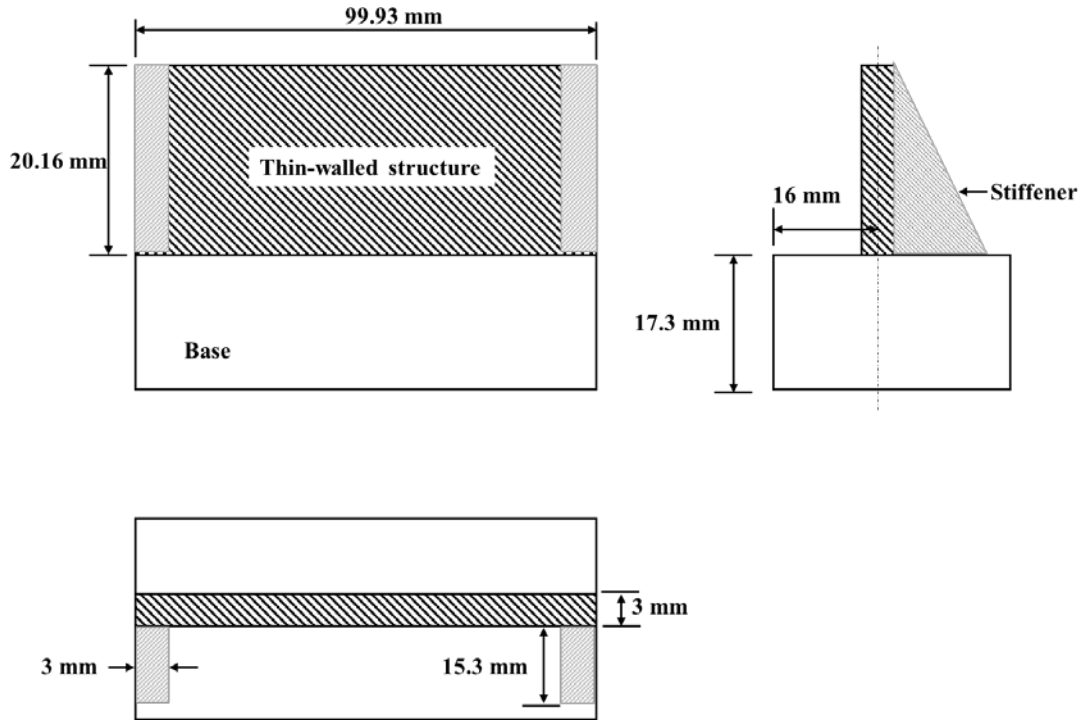


Figure 2.29: Two-dimensional (2D) detailed drawing of an aluminum Al-6061 thin-walled structure with clamped-clamped-clamped-free (CCCCF) boundary conditions.

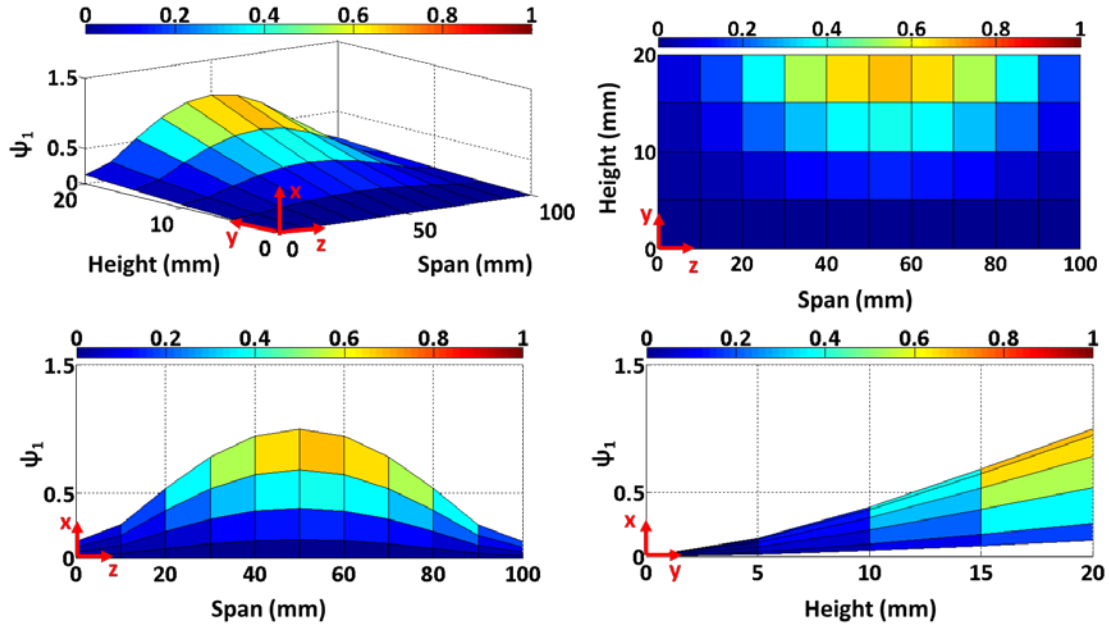


Figure 2.30: Predicted first mode shape, ψ_1 , with a natural frequency of 5821.9 Hz for the CCCF boundary condition.

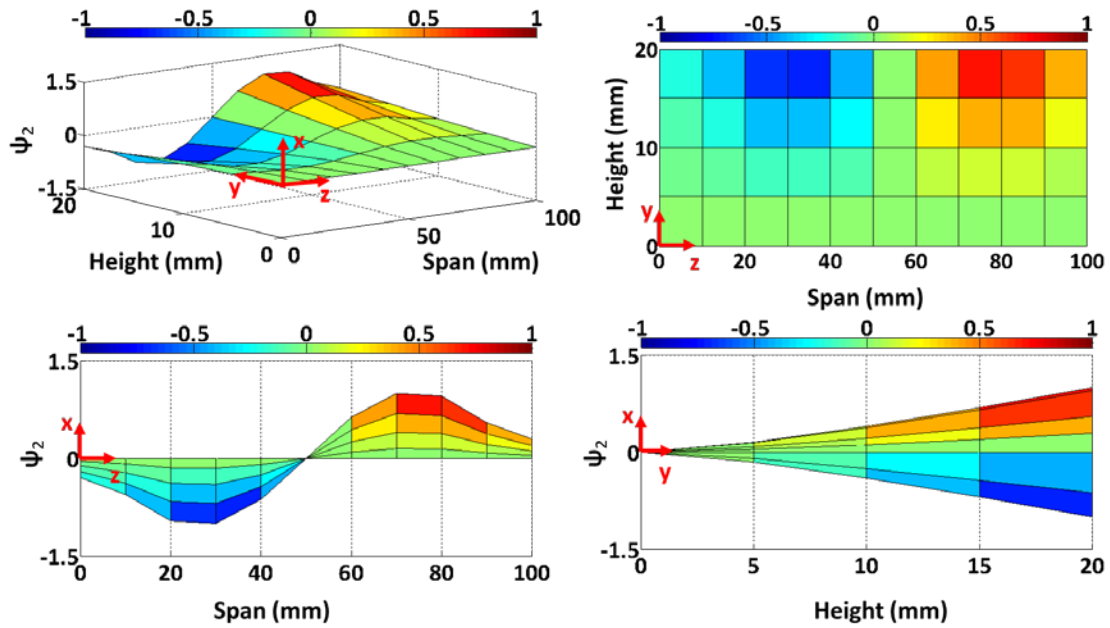
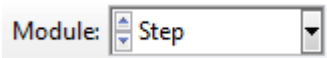


Figure 2.31: Predicted second mode shape, ψ_2 , with a natural frequency of 7598.1 Hz for the CCCF boundary condition.

2.2.4.2 Mode-based steady-state dynamic analysis

After extracting the natural frequencies and mode shapes, the mode-based steady-state dynamic analysis was used to calculate the steady-state dynamic linearized response of each system, i.e., the frequency response function (FRF) for harmonic excitation. As the name suggests, this step calculates the response based on the system's eigenvalues and eigenvectors and, therefore, requires that a natural frequency extraction procedure be performed prior to the steady-state dynamic analysis. The mode-based steady-state dynamic step is defined by specifying the frequency ranges of interest with a linear spacing and a bias parameter of 1. Also, the damping coefficient, i.e., the viscous damping ratio, is defined for a specified mode number and a concentrated nodal force is applied to the displacement degree of freedom at the location of most interest in the structure's response. These loads vary sinusoidally with time over a user-specified range of frequencies [30]. The steps to predict the mode-based steady-state analysis (FRF) of the system are provided in the following sections.


Step-VIII: Boundary condition and load

The model force is applied as a sinusoidal load in ABAQUS/CAE. To apply the load a new analysis, or step, is created. Switch to  *Step* from the

Module drop down box and then  *Create Step* so that a Create Step dialog box appears on screen. Input the following data.

- *Name*: Predicted FRF
- *Procedure type*: Linear perturbation, Steady-state dynamics, Modal

Press *Continue* and in the *Edit Step* dialog box select *Linear Scale* and *Use eigenfrequencies to subdivide each frequency range*. For the *Lower and Upper Frequency*,

enter the range such that the FRF can capture the lower (left side) and higher (right side) frequency of the desired range. For instance, if the first mode natural frequency is 500 Hz select lower range as 400 Hz and higher range as 600 Hz. For better resolution, use *Number of Points* as *Upper Frequency – Lower Frequency* with *Bias* factor of 1. Note that a larger number of points increases the simulation time and memory size. In the *Damping* tab, select *Direct modal - Use direct damping data* and enter the damping ratios for the corresponding modes (modal damping ratio). Apply the sinusoidal load at the desired location of the thin-wall feature. In Figures 2.26 to 2.28, 2.30, and 2.31, it is seen that the most flexible part of the thin-wall feature is the free edge. Therefore, the force is applied at this flexible free edge of the thin-wall structure. ABAQUS/CAE requires that the location used to apply the load and predict the FRF should be a point on the CAD model, but there are only four vertices/points available at the ends of the span length. To create the desired points, use the *Partition* and *Datum* operation to create vertices on the free edge. Switch to *Part* module and select *Datum* from the *Tools* menu and select *Offset from points*. Then select a point to create an offset and enter the desired (X, Y, Z) coordinate, e.g., (0.0, 0.0, -0.01). This creates the datum point in the negative Z direction with an offset value of 0.01 m. Note that the units should be constant throughout analysis. After creating the desired *Datum points*, use *Partition* from the *Tools* menu and select *Cell Type* and *Method* as *Define cutting plane*. Then select all cells, click *Point & Normal*, and select the created datum point for *the point* and the free edge for *the line* in the Y-Z plane. Select *Create Partition*. Then, to assign names to these datum points for convenience when assigning the load, select *Sets, Geometry* from the *Tools* menu and enter the desired name and select the created datum points. To apply the load, select  *Create Load* and enter the following data.

- *Name*: F1 (Desired name for load)
- *Step*: Predicted FRF
- *Procedure*: *Steady-state-dynamic, Modal*
- *Category*: *Mechanical*
- *Types for Selected Step*: *Concentrated force*

Press *Continue*. Select *Sets* and select the desired set name corresponding to the location of the force. In the Edit Load dialog box, select *Uniform Distribution* and enter 1+i0 (Force of 1N) in the *CF1* text box. *CF1*, *CF2*, and *CF3* are to be considered as (X, Y, and Z) axis and load of 1N applied at the desired location as it eliminates the need to normalize the FRF to the actual force level. Note that to determine the FRF, apply one load per simulation, but the sets created will help to determine the FRF at all these created sets.

Step-XI: Results

Once the simulation is completed, a message will be displayed in the Message area box. The results for the Mode-based steady-state analysis can be viewed by selecting the *Job* menu and *Results*. The Viewport window should appear on the screen. Navigate to *Options* in *Result* menu bar and select Real (default) or Imaginary *Complex Form* tab. ABAQUS/CAE displays the real or imaginary parts of the FRF and so the user has to navigate to the settings to switch between the real and imaginary part of the FRF. After the selection of the desired form of the FRF, go to the *Tools* menu bar and select *XY data* and then *Create*. The *Create XY Data* dialog box will appear; select *ODB field output* and press *Continue*. An *XY Data from ODB Field Output* dialog box will appear and, since the current analysis has two active steps, Natural Frequency Extraction step and Mode-based- steady-state dynamic step, the Natural Frequency Extraction step needs to be closed. Select *Active*

Steps/Frames on the top right of the *XY Data from ODB Field Output* dialog box and uncheck the step name that indicates *Time : Modal* and press OK to return to the *XY Data from ODB Field Output* dialog box. To plot the predicted FRF of the point/s created using the Datum and Partition in Step-VIII, select *Unique Nodal* in the *Position* drop down box and then check *U1* (*U1*, *U2*, and *U3* are the X, Y and Z coordinates) in the *U: Spatial displacement*. After selecting the direction of displacement in the *Variable* tab navigate to *Elements/Nodes* and selecting *Node sets* in the Selection Method, pick the desired node displayed in the following format: "Part name"-1."Location name". Also, select *Highlight items in viewport* to get a preview of the selected node of the model on the viewport and select *Plot* and *Dismiss* the *XY Data from ODB Field Output* dialog box. The viewport should now display the real or imaginary part of the FRF for the selected node location. The font and font size can be changed by selecting *XY Options* in the *Options* menu bar and select *Axis* and change the *Font* in the *Axes* tab. The same applies for the plot legend. The chart legend, bottom right of the plot, displays the Complex form type and node number corresponding to the selected location.

To save the result, navigate to *XY Data* in the *Result* tree, which contains the data points and name similar to the chart legend of the current plot. Rename it to the desired file name and then go to *Report* in the menu bar and select *XY*. In the *Report XY Data* dialog box, select the file. In the *Setup* tab and in the *File Name* text box, type the file name then select the directory to save the file. In the *Output Format* section, select *Separate table for each XY data*. This will create a separate column in the file for the x-y data and exit by pressing *OK* and save the file.

CHAPTER 3: EXPERIMENTAL VALIDATION

The dynamic characteristics of structure(s) are conventionally described using the complex-valued FRF, which defines the vibration output to force input ratio in the frequency domain. It represents the steady-state solution to the system differential equation of motion [31-33]. The dynamic response of the plate may be measured by modal testing. In this approach, an instrumented hammer is used to apply a known force, $F(t)$, to the structure and a transducer is used to measure the resulting response, $X(t)$. The FRF of the structure may be estimated from [32],

$$H(\omega) = \frac{X(\omega)}{F(\omega)}, \quad (3.1)$$

where $X(\omega)$ and $F(\omega)$ are the discrete Fourier transforms (DFT) of the response and force signals, respectively.

3.1 Experimental Setup

A commercial software package, MetalMax[®], was used to measure the plate FRFs. The input force was applied using a miniature modal hammer (PCB 084A17) with a steel tip (PCB 086E80 SN 33416) and the vibration response was measured using a laser Doppler vibrometer (Polytec OFV – 534 laser head with OFV-5000 controller). The OFV-5000 controller provides an output voltage proportional to the change in the velocity of the target.

In order to obtain FRFs that accurately reflect the predicted workpiece dynamics, it is important to very closely match the workpiece's boundary conditions to the finite

element analysis. Therefore, the workpiece was fixed to a heavy steel table using cyanoacrylate. This approximated a fixed boundary condition. The laser vibrometer was set at a stand-off distance of approximately 295 mm, which is consistent with the manufacturer-specified value [34] and the structure was impacted with the hammer at multiple locations. This setup provided controllable and repeatable dynamics. Figures 3.1 and 3.2 shows the experimental setup for measuring the plate dynamics.

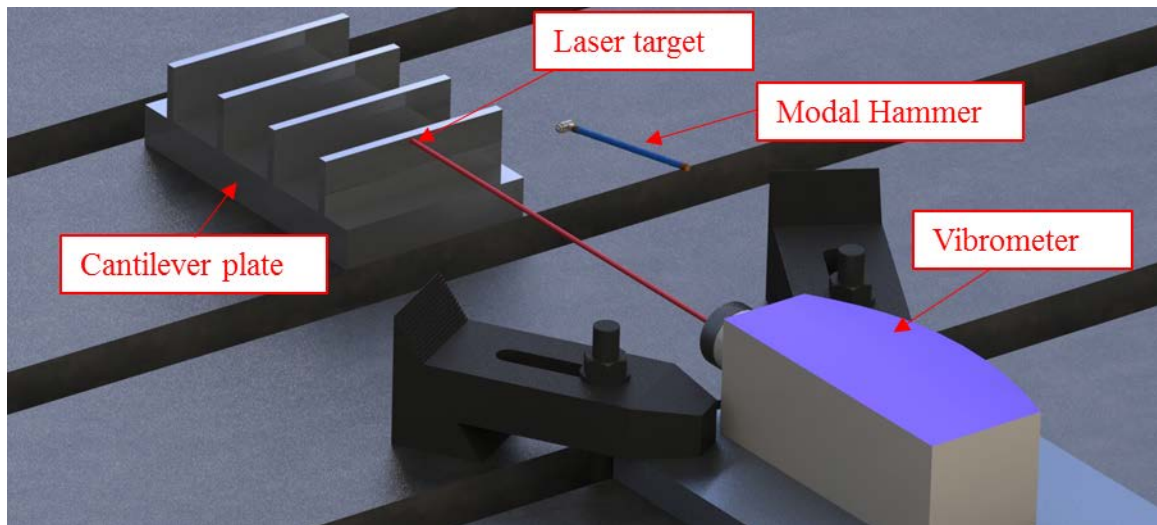


Figure 3.1: Schematic representation of cantilever rib FRF measurement setup using an impact hammer and laser vibrometer.

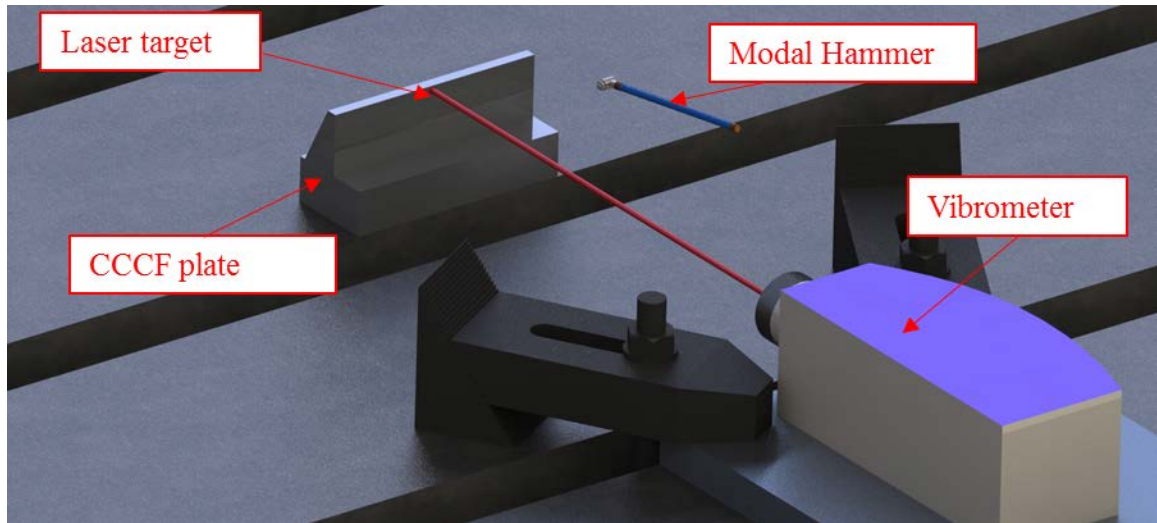


Figure 3.2: Schematic representation of CCCF rib FRF measurement setup using an impact hammer and laser vibrometer.

In modal testing, two signals are measured: the impulsive force and the vibration response. Any lack of synchronization in the time domain acquisition of these two signals results in a frequency-dependent phase error in the FRF. Given the time delay between the laser vibrometer and the hammer signals, a phase correction algorithm [31] was used to remove the corresponding phase error from the measured FRFs. Notice the changes with and without the phase correction in Figure 3.3. Also, MetalMax[©] uses a rectangular impulse window for force and an exponential window for the response. Because the damping is low for the parts tested in this study, the sampling time was increased to 30s. This enabled the full vibration response to be recorded without adding artificial damping through the exponential window. The phase error and windowing time are critical when measuring the dynamic response of a system because the complex FRF characterizes both the magnitude and phase of the structure's response to the force input.

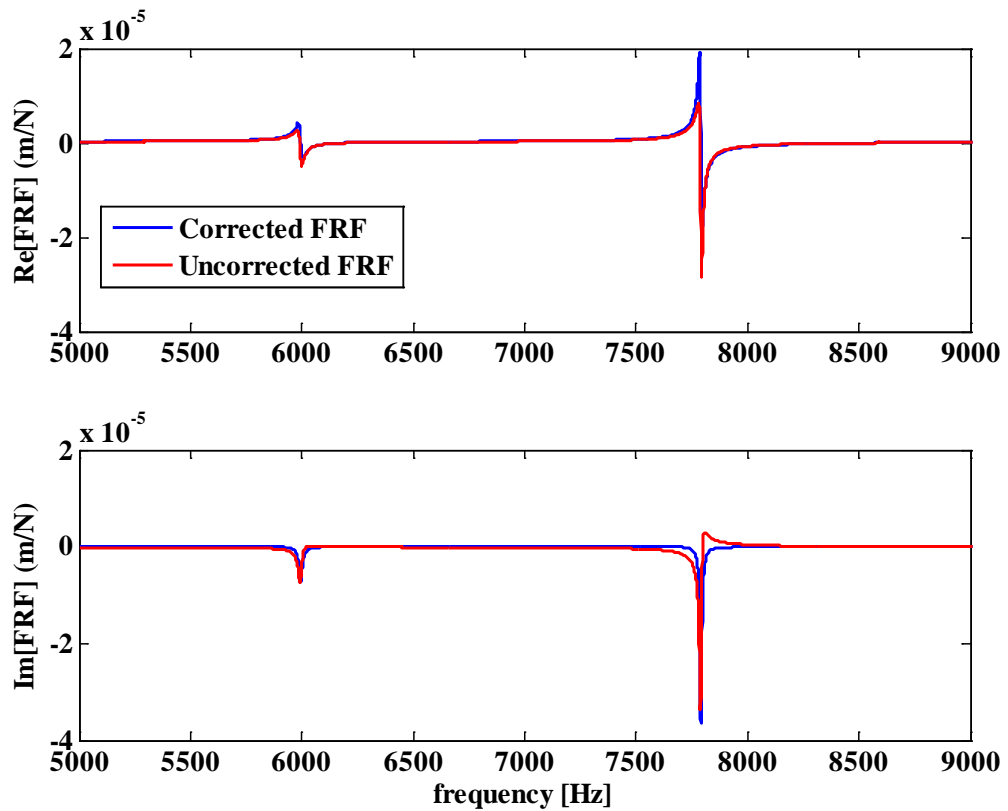


Figure 3.3: Comparison of the corrected and uncorrected FRF for a CCCF rib.

3.2 Comparison of Experimental and Measured Results

3.2.1 Mode Shapes

In order to measure mode shapes for cantilever and CCCF boundary conditions, the laser vibrometer target spot was located at an offset of 5mm from the top right corner of the plate and the structure was impacted with the hammer at multiple locations. Figures 3.4 to 3.8 show measured mode shapes for cantilever and CCCF boundary condition.

Table 3.1: Geometric dimensions for cantilever and CCCF thin-wall structure (all dimensions in mm).

Case	1	2
Geometry		
Length	101	99.93
Thickness	3.04	2.79
Height	20.1	20.16
Material	Al6061	Al6061

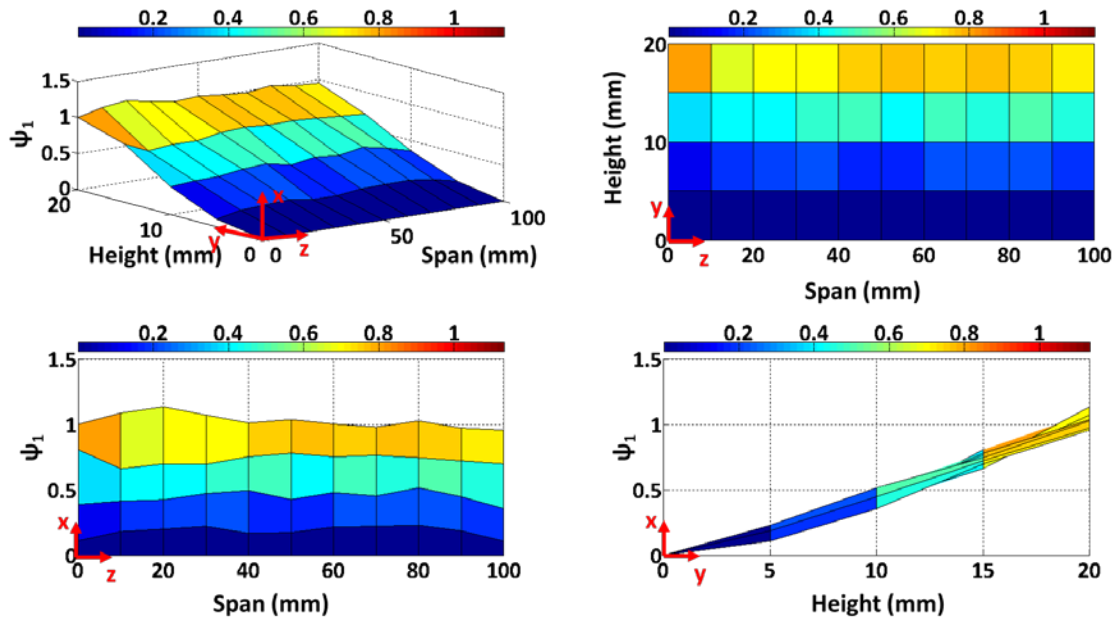


Figure 3.4: Measured first mode shape, ψ_1 , with a natural frequency of 5757.9 Hz for the cantilever boundary condition.

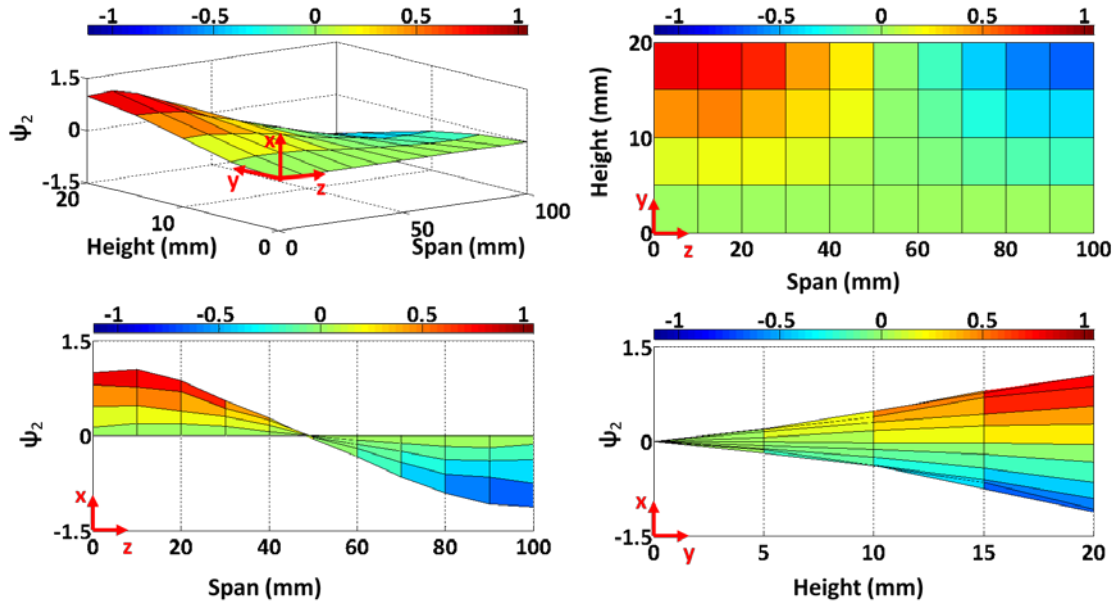


Figure 3.5: Measured second mode shape, ψ_2 , with a natural frequency of 6319.4 Hz for the cantilever boundary condition.

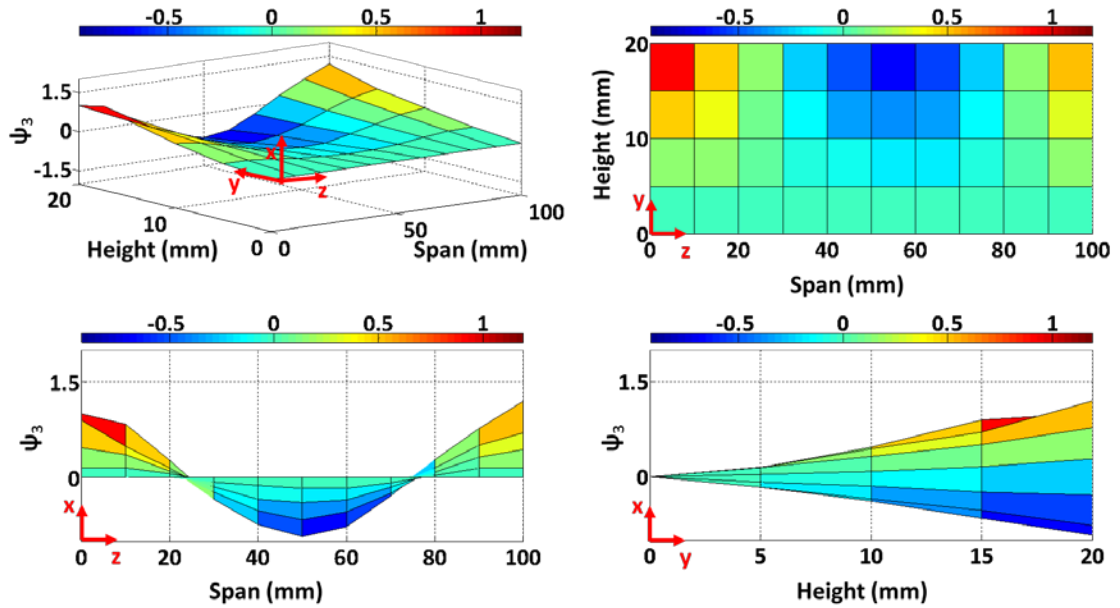


Figure 3.6: Measured third mode shape, ψ_3 , with a natural frequency of 7939.1 Hz for the cantilever boundary condition.

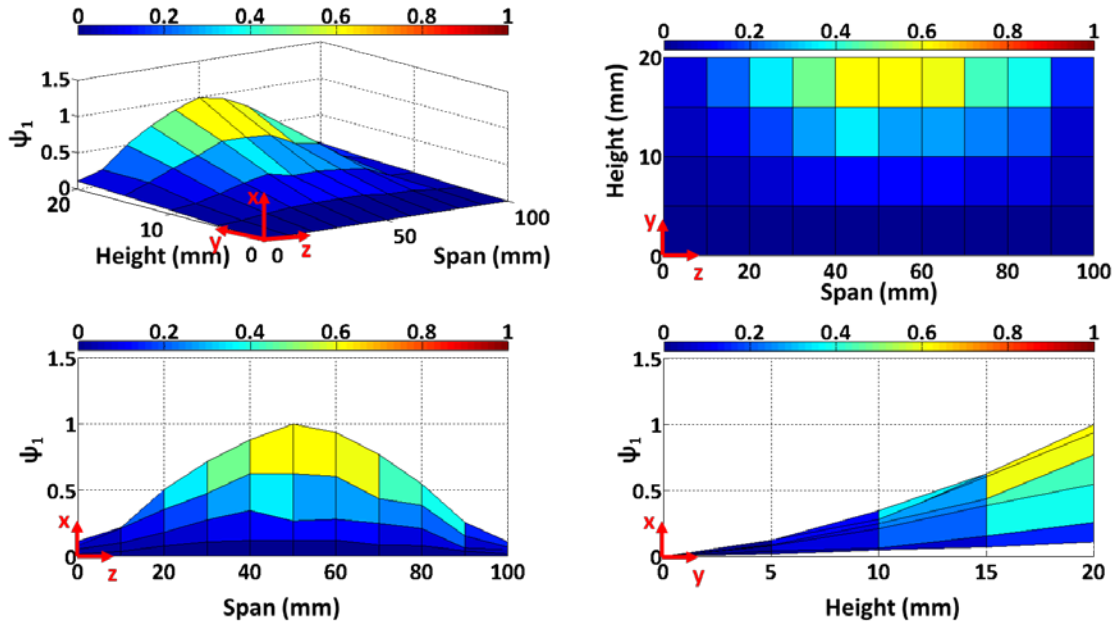


Figure 3.7: Measured first mode shape, ψ_1 , with a natural frequency of 5994.4 Hz for the CCCF boundary condition.

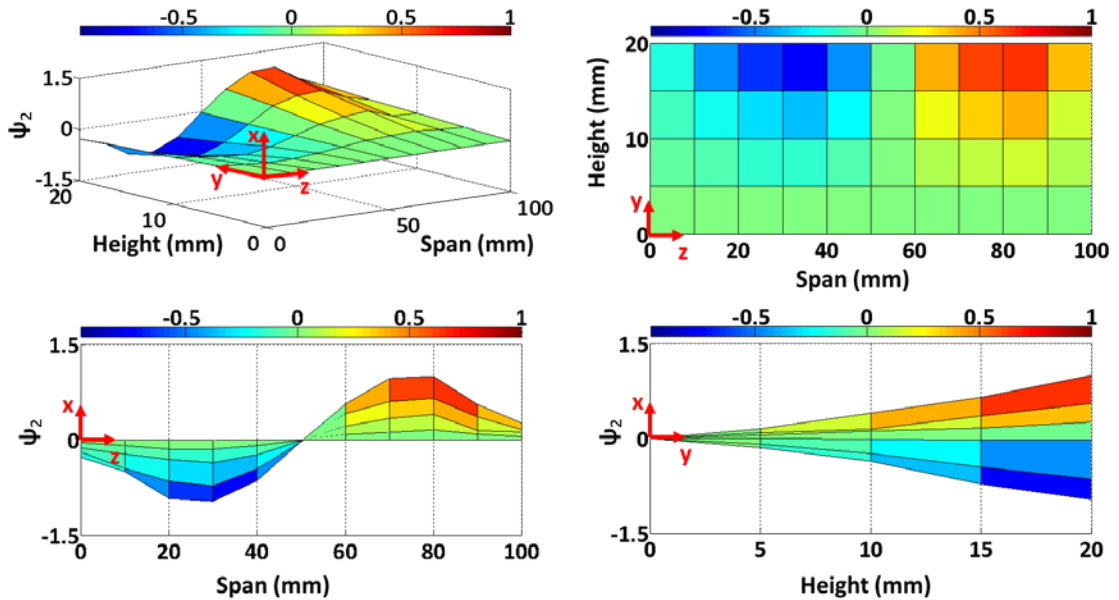


Figure 3.8: Measured second mode shape, ψ_2 , with a natural frequency of 7795.7 Hz for the CCCF boundary condition.

3.2.2 Frequency Response Function

Figure 3.9 shows the FRF of the free-edge of the CCCF plate. The measured and predicted first mode FRF was found to match within 10%.

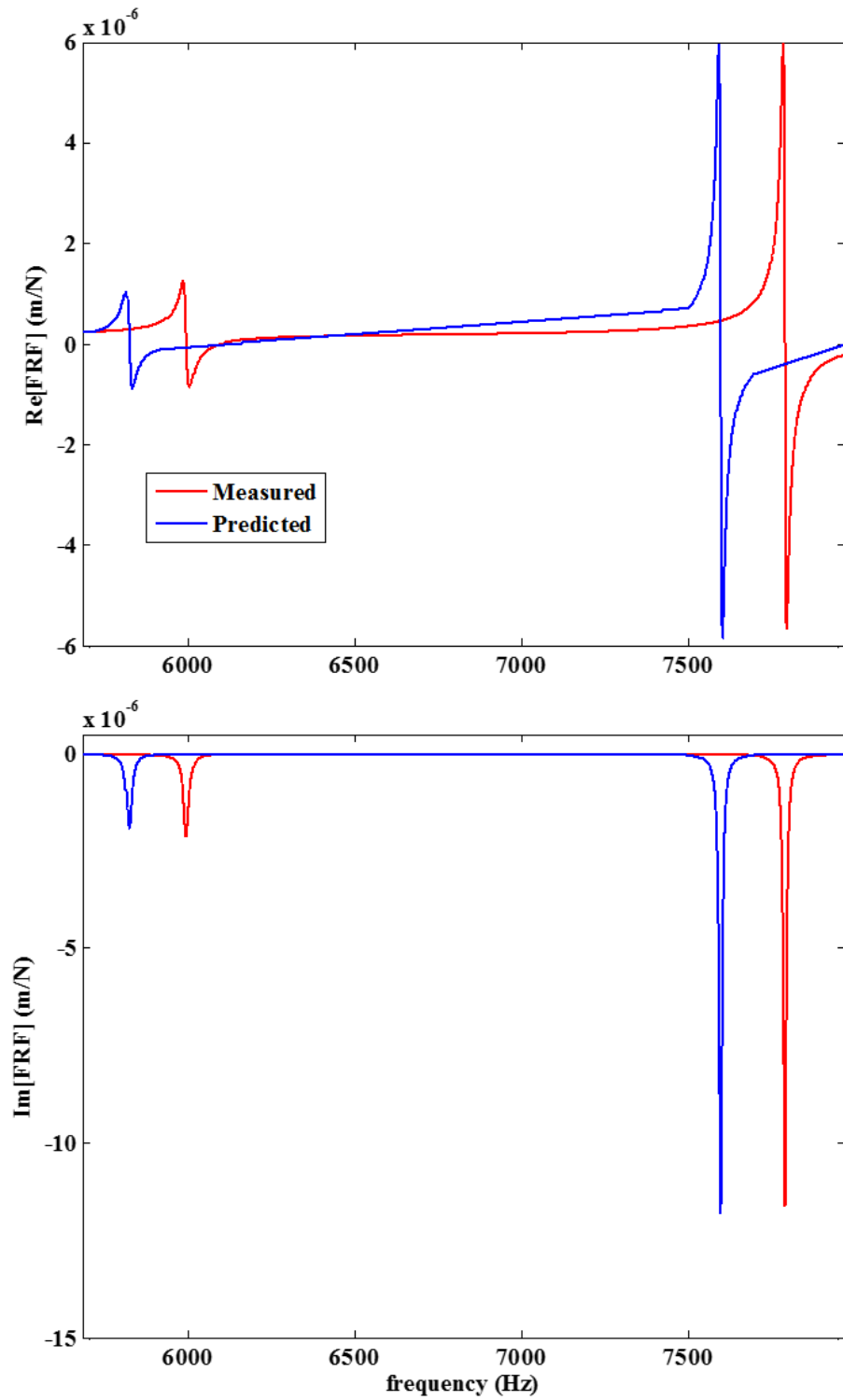


Figure 3.9: Comparison of the predicted and measured direct FRF for CCCF boundary condition at an offset of 45 mm from the center of the free edge.

3.2.3 Stiffness

Figures 3.10 and 3.11 show the stiffness at the free edge for cantilever and CCCF plates which was obtained using direct FRFs. The measured and predicted stiffness was found to match within 17%.

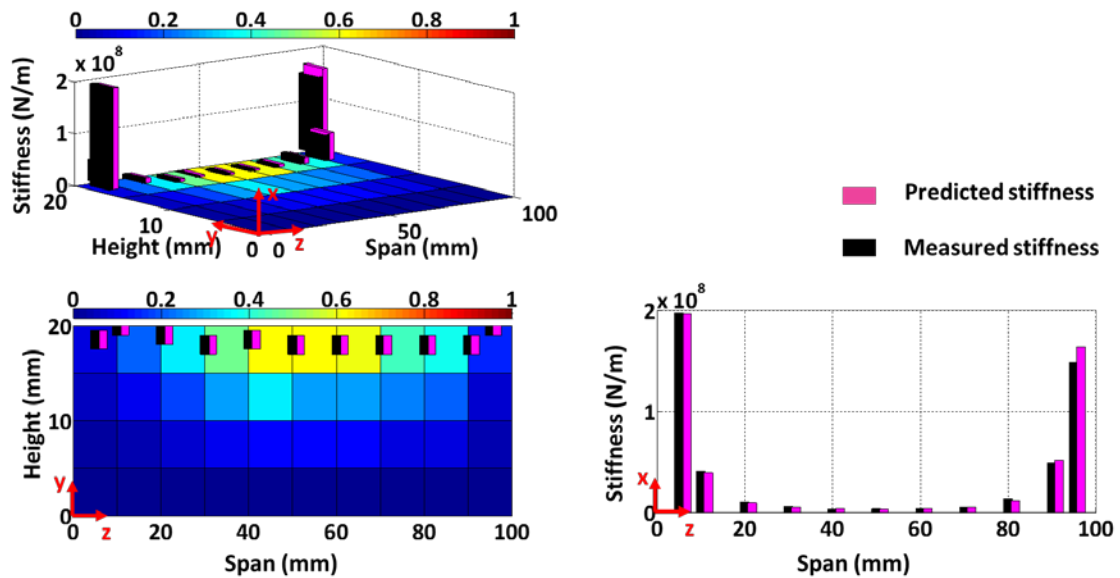


Figure 3.10: Comparison of the predicted and measured first mode stiffness at the free edge for the plate with CCCF boundary condition.

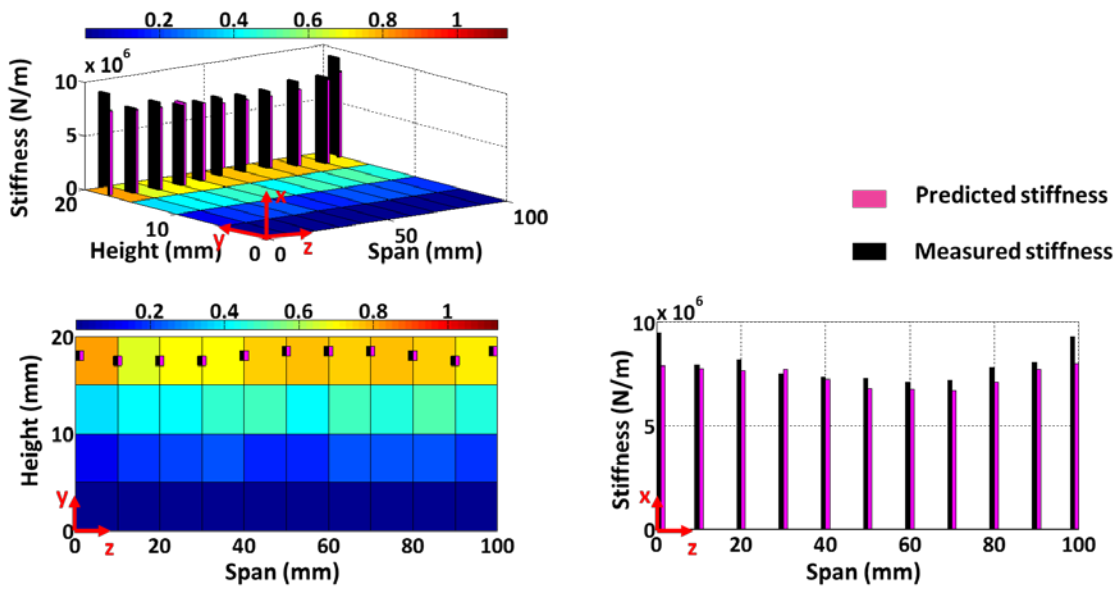


Figure 3.11: Comparison of the predicted and measured first mode stiffness at the free edge for the plate with cantilever boundary condition.

3.3 Test Geometries

Further analyses were conducted on other plate geometries with CCCF boundary conditions; see Figure 3.12 and Table 3.2. The minimum stiffness and its corresponding natural frequency (first mode) for these geometries are summarized in Table 3.3. Note that the original cantilever plate is case 1 and the original CCCF plate is case 2.

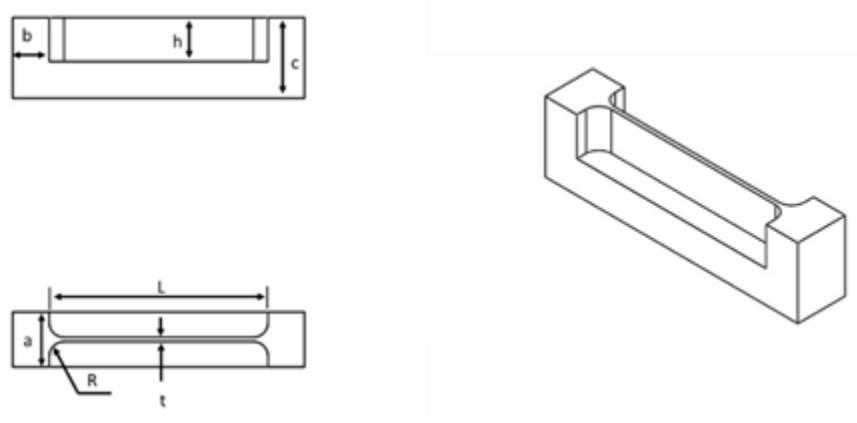


Figure 3.12: Dimensions for additional CCCF test geometries.

Table 3.2: Geometry and material for additional test geometries (all dimensions in mm).

Case \ Geometry	3	4	5	6	7
a	25	25	37.72	25	25
b	14.0	13.7	24.76	88.94	26.44
c	36.91	47.86	53.75	50.80	50.80
R	11.43	11.43	10	11.43	11.43
L	150	150	150	101.52	226.52
t	2.01	2.01	2.95	2.0	2.0
h	30	40	30	25.4	25.4
Material	Al6061	Al6061	Ti6Al4V	Al7075	Al7075

Table 3.3: Comparison of the predicted and measured first mode modal parameters at the center of the free edge for all test geometries.

Case Modal Parameters	1	2	3	4	5	6	7
Measured natural frequency, f_{n_m} (Hz)	5757.9	5994.4	2238.5	1468.7	3123.5	3424.1	2669.5
Predicted natural frequency, f_{n_p} (Hz)	5605.7	5822.1	2173.4	1415.2	3100.3	3630.7	2634.2
$(f_{n_m} - f_{n_p})/f_{n_m}$ x 100 %	2.7	2.9	2.9	3.6	0.7	-6.0	1.3
Measured modal stiffness, k_m (N/m) (x 10^6)	7.258	3.721	0.5311	0.302	2.6382	0.715	0.998
Predicted modal stiffness, k_p (N/m) (x 10^6)	6.700	3.406	0.55	0.29	2.5	0.7	0.997
$(k_m - k_p)/k_m$ x 100 %	6.8	8.5	-3.8	3.8	3.5	-4.5	0.1

CHAPTER 4: RESULTS AND DISCUSSION

The dynamic characteristics of the plate were predicted using finite element analysis and its accuracy was experimentally validated using impact tests. The tolerance intervals for all the test geometries were established to evaluate the repeatability of the experimental method for determining the dynamic characteristics. Quantitative effects of the mesh refinement and changes in length and fillet radius were evaluated using the predicted frequency response function described in Chapter 3. Using the numerical finite element modeling capability, the natural frequency and minimum stiffness for the first (most flexible) mode was evaluated over a range of lengths, thickness, and heights.

4.1 Repeatability

Repeat impact testing was performed on each test geometry in order to observe the variability in the dynamic parameters. A series of three impact tests were performed by gluing the workpiece to the steel table. The surfaces of the workpiece and the steel table were cleaned using acetone in order to ensure a proper surface contact between the two surfaces. Table 4.2 displays the \pm one standard deviation (68%), SD, in the first mode measured modal parameters for different test geometries recorded in Table 4.1.

Table 4.1: Geometric dimensions for additional test geometries (all dimensions in mm).

Case \ Geometry	1	2	3	4	5	6	7
<i>Length</i>	101	99.93	150	150	150	101.52	226.52
<i>Thickness</i>	3.04	2.79	2.01	2.01	2.95	2.0	2.0
<i>Height</i>	20.1	20.16	30	40	30	25.4	25.4

4.2 Mesh Density

In finite element analysis (FEA), the accuracy of the results and required computing time are determined in large part by the finite element size (mesh density). Finer mesh (small element size) models lead to highly accurate results, but require increased computing time. On the other hand, a FE model with coarser mesh may yield less accurate results even though the computing time is reduced. Due to its importance in generating the desired parameter lookup table, a mesh density study is presented. The goal is to select appropriate elements size so that the created models provide accurate FEA results (see Chapter 2 - Figure 2.22). In Chapter 3, in order to validate the experimental results, the mesh density along the thickness was made finer in comparison to the length and height of the FEA model. Therefore, this meshing strategy is used throughout the study and to generate the lookup table.

Table 4.2: First mode measured modal parameters for different test geometries carried out by series of three repeatability measurements.

Case 1					
<i>Modal Parameters</i>	<i>Trial 1</i>	<i>Trial 2</i>	<i>Trial 3</i>	<i>Mean</i>	<i>SD</i>
f_{n1} (Hz)	5777.7	5764.8	5774.7	5772.4	6.8
k_I (N/m) $\times 10^6$	10.115	12.658	13.831	12.201	0.189
ζ_I (%)	0.086	0.099	0.093	0.093	0.007
Case 2					
<i>Modal Parameters</i>	<i>Trial 1</i>	<i>Trial 2</i>	<i>Trial 3</i>	<i>Mean</i>	<i>SD</i>
f_{n1} (Hz)	6011.9	6005.1	6004.3	6007.1	4.2
k_I (N/m) $\times 10^6$	4.191	4.125	4.043	4.119	0.074
ζ_I (%)	0.177	0.216	0.216	0.203	0.022
Case 3					
<i>Modal Parameters</i>	<i>Trial 1</i>	<i>Trial 2</i>	<i>Trial 3</i>	<i>Mean</i>	<i>SD</i>
f_{n1} (Hz)	2251.4	2246.9	2243.8	2247.4	3.8
k_I (N/m) $\times 10^6$	1.157	1.093	0.971	1.074	0.094
ζ_I (%)	0.135	0.136	0.153	0.140	0.010
Case 4					
<i>Modal Parameters</i>	<i>Trial 1</i>	<i>Trial 2</i>	<i>Trial 3</i>	<i>Mean</i>	<i>SD</i>
f_{n1} (Hz)	1467.1	1466.4	1467.9	1467.1	0.8
k_I (N/m) $\times 10^6$	0.479	0.488	0.539	0.502	0.032
ζ_I (%)	0.234	0.234	0.208	0.225	0.015
Case 5					
<i>Modal Parameters</i>	<i>Trial 1</i>	<i>Trial 2</i>	<i>Trial 3</i>	<i>Mean</i>	<i>SD</i>
f_{n1} (Hz)	3113.6	3124.2	3105.2	3114.3	9.6
k_I (N/m) $\times 10^6$	4.772	4.855	4.605	4.744	0.127
ζ_I (%)	0.184	0.171	0.197	0.184	0.013
Case 6					
<i>Modal Parameters</i>	<i>Trial 1</i>	<i>Trial 2</i>	<i>Trial 3</i>	<i>Mean</i>	<i>SD</i>
f_{n1} (Hz)	3424.1	3423.3	3427.1	3424.8	2.0
k_I (N/m) $\times 10^6$	1.148	0.967	1.137	1.084	0.101
ζ_I (%)	0.167	0.234	0.178	0.193	0.036
Case 7					
<i>Modal Parameters</i>	<i>Trial 1</i>	<i>Trial 2</i>	<i>Trial 3</i>	<i>Mean</i>	<i>SD</i>
f_{n1} (Hz)	2669.5	2670.3	2669.5	2669.7	0.4
k_I (N/m) $\times 10^6$	4.515	4.479	4.759	4.584	0.153
ζ_I (%)	0.157	0.143	0.143	0.147	0.008

4.3 Comparison with Analytical Natural Frequency

Leissa [35, 36] provided an analytical expression for natural frequencies of rectangular plates with various boundary conditions, see equation 4.1:

$$f_{ij} = \frac{\lambda_{ij}^2}{2\pi a^2} \left[\frac{Eh^3}{12\gamma(1-\nu^2)} \right]^{1/2} ; i = 1, 2, 3 \dots ; j = 1, 2, 3 \dots \quad (4.1)$$

where a is the length, b is the width, and h is the thickness of the plate. Also, i is the number of half-waves in the mode shape along the horizontal axis, j is the number of half-waves in the mode shape along vertical axis, γ is the mass per unit area of the plate (ρh for a plate of a material with density ρ), λ_{ij} is the dimensionless frequency parameter of rectangular plates as a function of the boundary conditions applied at the edges of the plate (see Table 4.3), the aspect ratio (a/b) of the plate, and, in some cases, Poisson's ratio (ν). It has been found that λ_{ij} is independent of Poisson's ratio unless one or two edges of the rectangular plate are free. The dimensionless frequency parameter, λ_{11} , in Table 4.3 is a function of a Poisson's ratio of 0.3. However, the Poisson's ratio used for the finite element analysis is 0.33 for aluminum and 0.342 for titanium test geometries.

Table 4.3: Dimensionless frequency parameters of rectangular plate for analytical frequency.

λ_{11}^2		
Aspect ratio (a/b)	First mode sequence	
	CCCF Plate	Cantilever Plate
0.4	22.58	3.511
2/3	23.02	3.502
1.0	24.02	3.492
1.5	26.73	3.477
2.5	37.66	3.456

The first natural frequency for a CCCF plate with an aspect ratio greater than 2.5 (see Table 4.3) was evaluated using a computer program. The dimensionless frequency parameter was calculated using a curve fit to the parameters in Table 4.3:

$$f(x) = (px)^2 - qx + r \quad (4.2)$$

where p , q , and r are the coefficients with 95% confidence bounds. The coefficients for Equation 4.2 are shown in Table 4.4 and the curve fitting plot is shown in Figures 4.1 and 4.2. A comparison between the FEA, measured, and analytical first mode natural frequencies is provided in Table 4.5.

Table 4.4: Coefficients for curve fitting.

Coefficients	Cantilever plate	CCCF plate
p	0.06602	1.827
q	0.03894	2.551
r	3.526	23.15

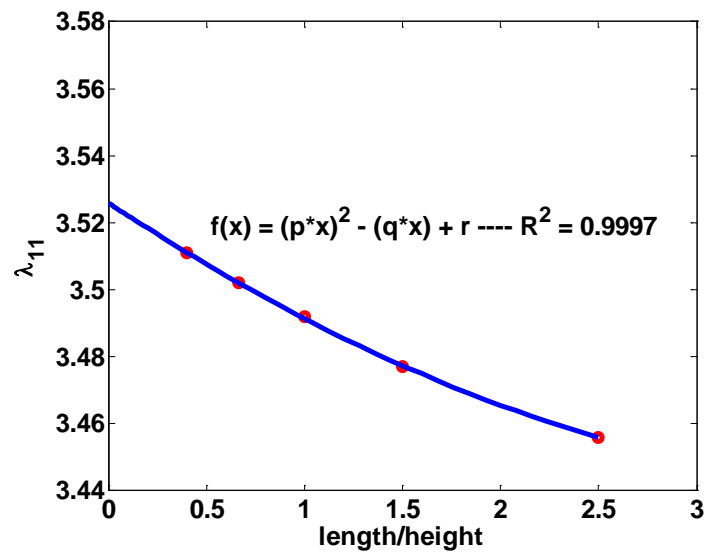


Figure 4.1: The resulting plot displays the aspect ratio (red circle) and curve fitting (blue line) for the cantilever plate.

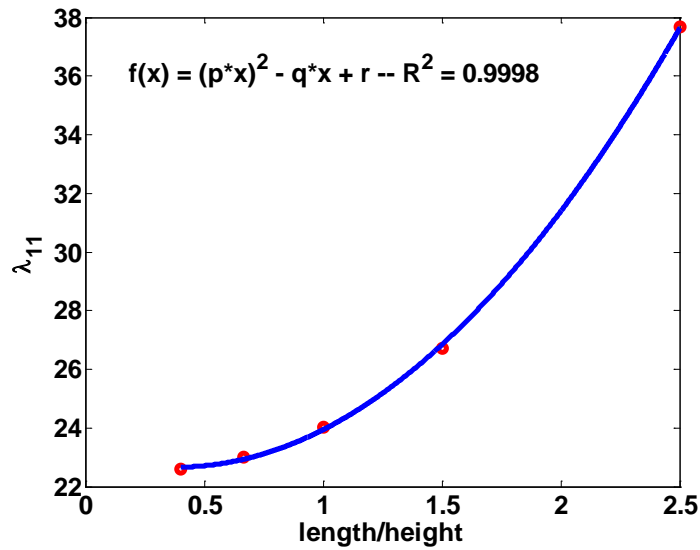


Figure 4.2: The resulting plot displays the aspect ratio (red circle) and curve fitting (blue line) for the CCCF plate.

Table 4.5: Comparison of the analytical, predicted and measured first mode natural frequency for all test geometries.

Modal Parameters	Case	1	2	3	4	5	6	7
	Measured natural frequency, f_{n_m} (Hz)		5757.9	5994.4	2238.5	1468.7	3123.5	3424.1
Analytical natural frequency, f_{n_a} (Hz)		6488	6921.8	2050.9	1322.7	3049	3161.9	2547.8
Predicted natural frequency, f_{n_p} (Hz)		5605.7	5822.1	2173.4	1415.2	3100.3	3630.7	2634.2
$(f_{n_m} - f_{n_a})/f_{n_m}$ x 100 %		-12.7	-15.5	8.4	9.9	2.4	7.7	4.6
$(f_{n_m} - f_{n_p})/f_{n_m}$ x 100		2.7	2.9	2.9	3.6	0.7	-6.0	1.32

4.4 Grid and Interpolation for Natural Frequency and Stiffness

Finally, using FEA, the minimum stiffness and corresponding natural frequency (for the first mode) were evaluated for changes in length ranging from 150 mm to 1450 mm, thickness from 1.5 mm to 15.5 mm, and height from 12 mm to 152 mm. These trends were combined into a lookup table that can be used to identify the natural frequency and minimum rib stiffness for any selected geometry; see Figures 4.3 to 4.6. A computer program was used to develop the lookup table by interpolation. The program returns interpolated values of stiffness and natural frequency as a function of three input geometry variables (height, thickness, and length) for titanium workpieces using spline interpolation. Using the interpolated natural frequency and stiffness values, the workpiece dynamics can be defined and, using milling stability methods, stable machining parameters may be identified. The MATLAB code is given in APPENDIX A.

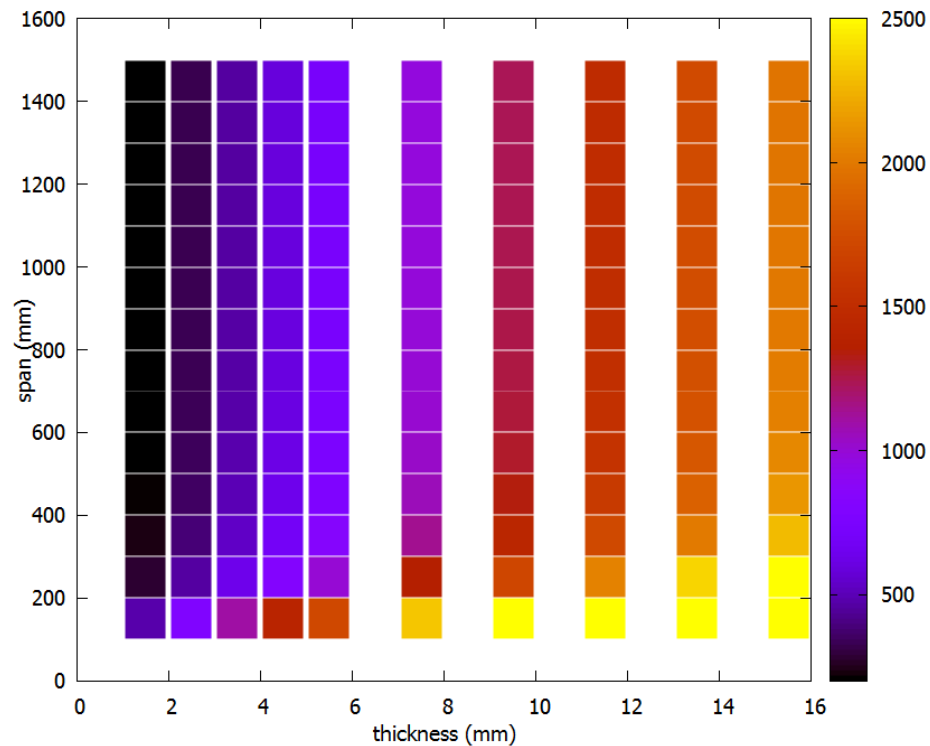


Figure 4.3: The plot displays the natural frequency values for a 72 mm tall CCCF plate.

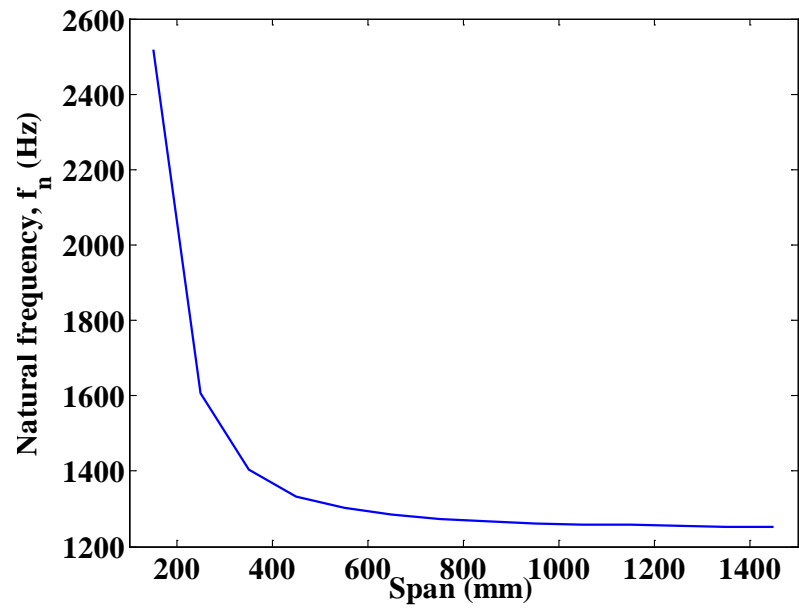


Figure 4.4: The plot displays the natural frequency values for a 7.5 mm thick and 72 mm tall CCCF plate.

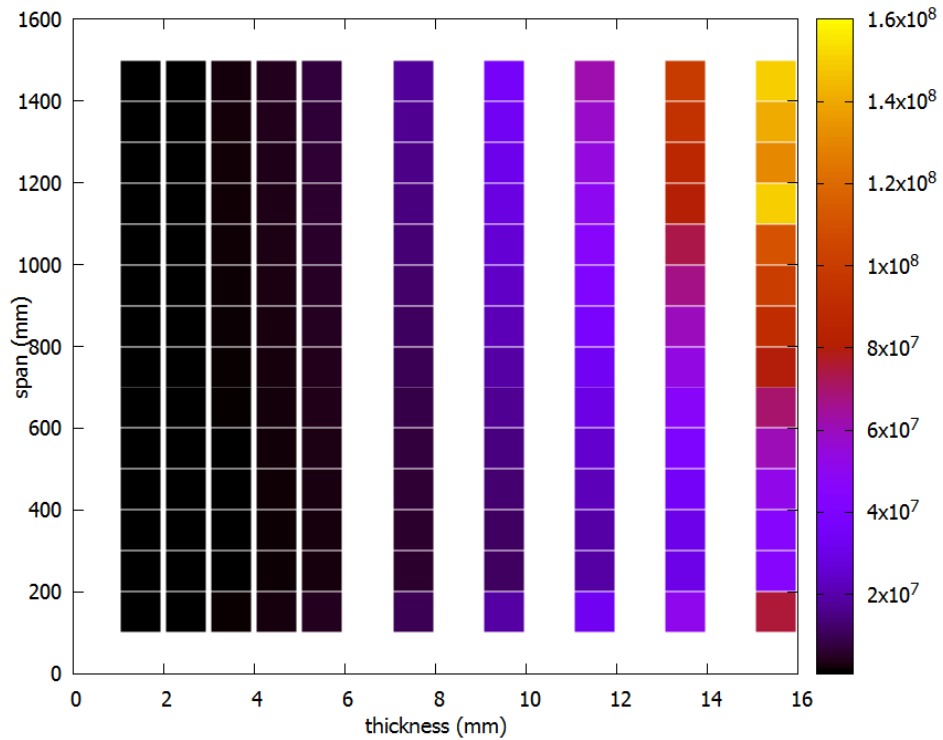


Figure 4.5: The plot displays the minimum stiffness values for a 72 mm high CCCF plate.

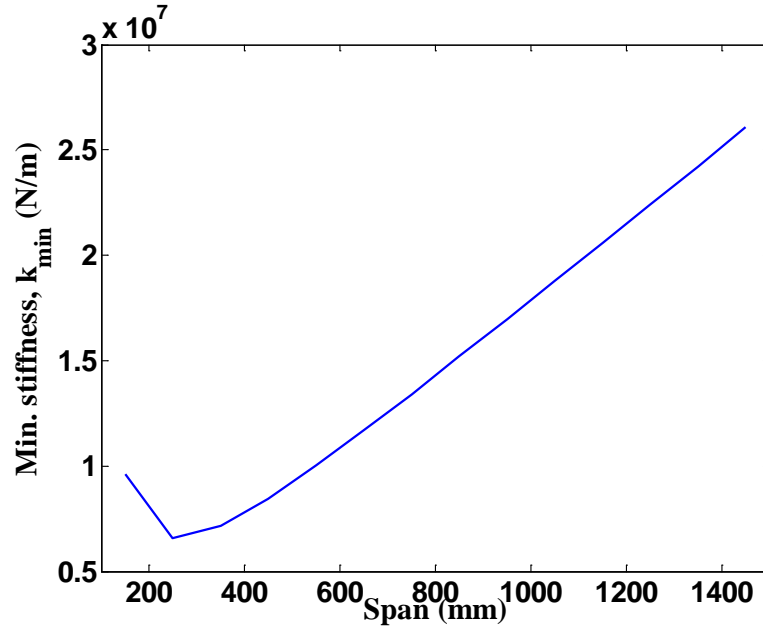


Figure 4.6: The plot displays the stiffness values for a 7.5 mm thick and 72 mm tall CCCF plate.

Table 4.6: Comparison of the modal parameters for CCCF plate with respect to increase in span length.

Modal Parameters	Case	
	6	7
Measured natural frequency, f_{n_m} (Hz)	3424.1	2669.5
Predicted natural frequency, f_{n_p} (Hz)	3630.7	2634.2
$(f_{n_m} - f_{n_p})/f_{n_m} \times 100 \%$	-6.0	1.3
Measured minimum stiffness, k_m (N/m) $\times 10^6$	0.715	0.998
Predicted modal stiffness, k_p (N/m) ($\times 10^6$)	0.747	0.997
$(k_m - k_p)/k_m \times 100 \%$	-4.5	0.1
Measured modal mass, m_m (kg)	0.0015	0.0035
Predicted modal mass, m_p (kg)	0.0014	0.0036
$(m_m - m_p)/m_m \times 100 \%$	6.7	-2.9
Damping coefficient, c (N-s/m)	0.111	0.170
$(c_m - c_p)/c_m \times 100 \%$	1.8	-0.6
Damping ratio, ζ (%)	0.170	0.143

Based on, Figure 4.6 it was observed that an increase in the span length (with other parameters fixed) results in an increase in the stiffness of the CCCF plate. This observation was verified by conducting an impact test on the case 6 and 7 test geometries and is reported in Table 4.6. The longer span rib (7) has a higher stiffness than the shorter span rib (6).

CHAPTER 5: SUMMARY AND CONCLUSION

In this work, a semi-analytical model for thin-plate dynamics was developed that considers first mode natural frequency and its corresponding minimum stiffness. The analysis were carried out using ABAQUS/EXPLICIT. The motivation behind this study was to enable high precision machining of thin features in hard-to-machine materials at high efficiency and low cost. A brief introduction to thin-wall machining and a literature survey was presented first. This was followed by the current techniques used for thin-wall machining. The analyses were carried out as two cases. First, the thin-wall with cantilever boundary condition was considered to understand its response to anticipated cutting forces. Second, the thin-wall with clamped-clamped-clamped-free boundary condition was modeled by using stiffeners.

A comparison of predicted and measured natural frequencies, stiffness values, and mode shapes showed good agreement for thin-walled structures with cantilever and clamped-clamped-clamped-free boundary conditions. In both cases, the first mode was taken to be the most flexible mode and, therefore, the focus was on studying the flexible first mode corresponding natural frequency and stiffness as various geometric parameters were varied. Further analyses were conducted on other plate geometries with clamped-clamped-clamped-free boundary conditions.

Repeat impact tests were performed in order to observe the variability in the dynamic parameters. A series of three test were performed by gluing the test geometries to the steel

table and the \pm one standard deviation (68%) was calculated. Results indicated acceptable repeatability in the dynamic parameters using the experimental approach. Furthermore, it was determined that the mesh resolution, especially along the thickness, is critical to predicting dynamic parameters.

An analytical natural frequency expression [36] was used to compare the predicted and measured natural frequency. The analytical natural frequency was found to be comparable with predicted (finite element analysis) and measured natural frequencies. The error deviated by up to -15.5% between analytical and measured natural frequencies and -6.0% between analytical and predicted natural frequencies.

Finally, using the numerical finite element modeling capability, the natural frequency and minimum stiffness for the first (most flexible) mode was evaluated over a range of lengths, thicknesses, and heights. These trends were combined into a lookup table that can be used to identify the natural frequency and minimum rib stiffness for the selected geometry. Using the interpolated natural frequency and stiffness values, the workpiece dynamics can be defined and, using milling stability methods, stable machining parameters may be identified.

REFERENCES

- [1] S. Smith and D. Dvorak, "Tool path strategies for high speed milling aluminum workpieces with thin webs," *Mechatronics*, vol. 8, pp. 291-300, 1998.
- [2] S. Smith and J. Tlusty, "Current trends in high-speed machining," *Journal of Manufacturing Science and Engineering*, vol. 119, pp. 664-666, 1997.
- [3] S. Smith, W. Winfough, and J. Halley, "The effect of tool length on stable metal removal rate in high speed milling," *CIRP Annals-Manufacturing Technology*, vol. 47, pp. 307-310, 1998.
- [4] J. Tlusty, S. Smith, and W. Winfough, "Techniques for the use of long slender end mills in high-speed milling," *CIRP Annals-Manufacturing Technology*, vol. 45, pp. 393-396, 1996.
- [5] J.-S. Tsai and C.-L. Liao, "Finite-element modeling of static surface errors in the peripheral milling of thin-walled workpieces," *Journal of Materials Processing Technology*, vol. 94, pp. 235-246, 1999.
- [6] J. Tlusty and M. Polacek, "1963The stability of the machine tool against self excited vibration in machining," in *Proc. Conf. on International Research in Production Engineering, Pittsburgh, PA, USA*. pp, pp. 465-474.
- [7] S. Tobias, "Machine tool vibration research," *International Journal of Machine Tool Design and Research*, vol. 1, pp. 1-14, 1961.
- [8] J. Tlusty and F. Koenigsberger, "Machine tool structures," ed: Pergamon Press Oxford, 1970.
- [9] I. Minis and R. Yanushevsky, "A new theoretical approach for the prediction of machine tool chatter in milling," *Journal of engineering for industry*, vol. 115, pp. 1-8, 1993.
- [10] I. Minis, R. Yanushevsky, A. Tembo, and R. Hocken, "Analysis of linear and nonlinear chatter in milling," *CIRP Annals-Manufacturing Technology*, vol. 39, pp. 459-462, 1990.
- [11] A.-C. Lee and C.-S. Liu, "Analysis of chatter vibration in the end milling process," *International Journal of Machine Tools and Manufacture*, vol. 31, pp. 471-479, 1991.
- [12] A.-C. Lee, C.-S. Liu, and S.-T. Chiang, "Analysis of chatter vibration in a cutter-workpiece system," *International Journal of Machine Tools and Manufacture*, vol. 31, pp. 221-234, 1991.

- [13] Y. Altıntaş and E. Budak, "Analytical prediction of stability lobes in milling," *CIRP Annals-Manufacturing Technology*, vol. 44, pp. 357-362, 1995.
- [14] U. Bravo, O. Altuzarra, L. L. De Lacalle, J. Sánchez, and F. Campa, "Stability limits of milling considering the flexibility of the workpiece and the machine," *International Journal of Machine Tools and Manufacture*, vol. 45, pp. 1669-1680, 2005.
- [15] H. Lacerda and V. Lima, "Evaluation of cutting forces and prediction of chatter vibrations in milling," *Journal of the Brazilian Society of Mechanical Sciences and Engineering*, vol. 26, pp. 74-81, 2004.
- [16] S. Merdol and Y. Altintas, "Multi frequency solution of chatter stability for low immersion milling," *Journal of Manufacturing Science and Engineering*, vol. 126, pp. 459-466, 2004.
- [17] E. Solis, C. Peres, J. Jimenez, J. Alique, and J. Monje, "A new analytical-experimental method for the identification of stability lobes in high-speed milling," *International Journal of Machine Tools and Manufacture*, vol. 44, pp. 1591-1597, 2004.
- [18] E. Budak and Y. Altintas, "Analytical prediction of chatter stability in milling—part I: general formulation," *Journal of Dynamic Systems, Measurement, and Control*, vol. 120, pp. 22-30, 1998.
- [19] E. Budak and Y. Altintas, "Analytical prediction of chatter stability in milling—part II: application of the general formulation to common milling systems," *Journal of Dynamic Systems, Measurement, and Control*, vol. 120, pp. 31-36, 1998.
- [20] F. Campa, L. L. de Lacalle, A. Lamikiz, and J. Sanchez, "Selection of cutting conditions for a stable milling of flexible parts with bull-nose end mills," *Journal of Materials Processing Technology*, vol. 191, pp. 279-282, 2007.
- [21] V. Thévenot, L. Arnaud, G. Dessenin, and G. Cazenave-Larroche, "Influence of material removal on the dynamic behavior of thin-walled structures in peripheral milling," *Machining Science and Technology*, vol. 10, pp. 275-287, 2006.
- [22] S. Seguy, F. J. Campa, L. N. Lopez de Lacalle, L. Arnaud, G. Dessenin, and G. Aramendi, "Toolpath dependent stability lobes for the milling of thin-walled parts," *International Journal of Machining and Machinability of Materials*, vol. 4, pp. 377-392, 2008.
- [23] V. Thevenot, L. Arnaud, G. Dessenin, and G. Cazenave-Larroche, "Integration of dynamic behaviour variations in the stability lobes method: 3D lobes construction and application to thin-walled structure milling," *The International Journal of Advanced Manufacturing Technology*, vol. 27, pp. 638-644, 2006.

- [24] S. Herranz, F. Campa, L. L. De Lacalle, A. Rivero, A. Lamikiz, E. Ukar, *et al.*, "The milling of airframe components with low rigidity: a general approach to avoid static and dynamic problems," *Proceedings of the Institution of Mechanical Engineers, Part B: Journal of Engineering Manufacture*, vol. 219, pp. 789-801, 2005.
- [25] D. Montgomery, Y. Altintas, and E. Budak, "Dynamic peripheral milling of flexible structures," *Trans. ASME, J. Eng. Ind*, vol. 114, pp. 137-145, 1992.
- [26] E. Budak and Y. Altintas, "Modeling and avoidance of static form errors in peripheral milling of plates," *International Journal of Machine Tools and Manufacture*, vol. 35, pp. 459-476, 1995.
- [27] W. Kline, R. DeVor, and I. Shareef, "The prediction of surface accuracy in end milling," *Journal of Engineering for Industry*, vol. 104, pp. 272-278, 1982.
- [28] S. Smith, R. Wilhelm, B. Dutterer, H. Cherukuri, and G. Goel, "Sacrificial structure preforms for thin part machining," *CIRP Annals-Manufacturing Technology*, vol. 61, pp. 379-382, 2012.
- [29] Z.-Q. Qu, *Model order reduction techniques with applications in finite element analysis*: Springer Science & Business Media, 2013.
- [30] A. U. Manual, "Version 6.13-2 Dassault Systmes Simulia Corp.," ed. Providence, Rhode Island, USA, 2013.
- [31] V. Ganguly and T. L. Schmitz, "Phase correction for frequency response function measurements," *Precision Engineering*, vol. 38, pp. 409-413, 2014.
- [32] T. L. Schmitz and K. S. Smith, *Mechanical vibrations: modeling and measurement*: Springer Science & Business Media, 2011.
- [33] D. Ewins, *Modal Testing: Theory, Practice, and Application*: Research Studies Press, 2000.
- [34] V. C. U. Manual, "OFV-5000, Polytec," ed: Inc.
- [35] R. Blevins, "Formulas for natural frequency and mode shape, 1979," *Kreiger Publ. Comp., New York*.
- [36] A. W. Leissa, "The free vibration of rectangular plates," *Journal of Sound and vibration*, vol. 31, pp. 257-293, 1973.

APPENDIX A: GRID AND INTERPOLATION FOR NATURAL FREQUENCY AND STIFFNESS MATLAB CODE

```

% {
Grid and interpolation for natural frequency and stiffness

Created by Joyson Menezes and Kadir Kiran

This code inputs 10 by 14 by 15 matrix each of natural frequency and
minimum stiffness data which is predicted using ABAQUS/Standard 6.13
and performs interpolation of a function of three geometry variables
(height, thickness, and length) at specific query points using
spline interpolation.
% }

%Clear screen, variables, and figures.
clc
close all
clear all

%% INPUT GEOMETRIC DATA

%Enter the span length for the thin-plate
prompt_length = 'Please enter a span length for the thin-plate ranging from 150.0 to 1450.0
mm: \n ';
L = input(prompt_length);%if the entered length is outside the given limit an error message
will be displayed
while L <150.00 || L >1450.00
    clear all
    error('All values for length are outside the limit')%Error message
end
Length = L;

%Enter the thickness for the thin-plate in mm
prompt_thk = 'Please enter a thickness for the thin-plate ranging from 1.50 to 15.5 mm: \n';
thk = input(prompt_thk);
while thk <1.50 || thk >15.0 %if the entered thickness is outside the given limit an error
message will be displayed
    clear all
    error('All values for thickness are outside the limit')%Error message
end
Thickness = thk;

%Enter the height for the thin-plate in mm
prompt_ht = 'Please select a height for the thin-plate ranging from 12 to 152 mm: \n ';

```

```

Ht = input(prompt_ht);
while Ht <12.00 || Ht >152.00%if the entered height is outside the given limit an error
message will be displayed
    clear all
    error('All values for height are outside the limit')%Error message
end
Height = Ht;

%Returns interpolated natural frequency and min. stiffness
[Nf,MS] = interpolation_function(Length,Thickness,Height);

function [NF,MS] = interpolation_function(Len,thk,Ht)
% function to interpolate the natural frequency and min. stiffness using
% spline method

% load the 3D array of nat. freq. for height
load('nat_freq_height.mat');

% load the 3D array of min. stiffness for height
load('min_stiff_height.mat');

% Array holding the length, height and thickness
ht=[12:10:152]; %height(mm)
l=150:100:1450; %length(mm)
t=[1.5:1:5.5 7.5:2:15.5]; %thickness(mm)

% 3D array holding the natural frequency and minimum stiffness
th_nf=zeros(length(ht),length(l),length(t));
th_ms=zeros(length(ht),length(l),length(t));
for i=1:length(t)
    for j=1:length(l)
        for k=1:length(ht)
            th_nf(k,j,i)=h_nf(i,j,k);%3D array for natural frequency
            th_ms(k,j,i)=h_ms(i,j,k);%3D array for minimum stiffness
        end
    end
end
end

% Building mesh grid
h_i=[12:1:152];
l_i=[150:5:1450];
t_i=[1.5:1:5.5 7.5:2:15.5];

[L,H,T]=meshgrid(l_i,h_i,t_i);

```

```
% Interpolation function

% natural frequency
n_f=@(L,H,T)interp3(l,ht,t,th_nf,L,H,T,'spline');

% Minimum stiffness
m_s=@(L,H,T)interp3(l,ht,t,th_ms,L,H,T,'spline');

NF = n_f(Len,Ht,thk);%Interpolated natural frequency
MS = m_s(Len,Ht,thk);%Interpolated min. stiffness
end
```